Cell Reports
Physical Science

CellPress
OPEN ACCESS

Review

Research status and prospects of dynamic perception and quantitative detection sensors for icing characteristics

Han Shi,[1] Mengjie Song,[1,*] Xuan Zhang,[1] Long Zhang,[1] Keke Shao,[1] Zekang Zhen,[1] Runmiao Gao,[1] Christopher Yu Hang Chao,[2] Dong Rip Kim,[3] Xian Yi,[4] Bin Chen,[5] Bing Huang,[6] You Zhou,[7] Zhenyu Du,[8] and Zhiqiang Xu[9]

[1]Department of Energy and Power Engineering, School of Mechanical Engineering, Beijing Institute of Technology, Beijing, China
[2]Department of Building Environment and Energy Engineering and Department of Mechanical Engineering, The Hong Kong Polytechnic University, Hong Kong, China
[3]School of Mechanical Engineering, Hanyang University, Seoul, Republic of Korea
[4]China Aerodynamics Research and Development Center, Mianyang, China
[5]College of Electronic Information and Automation, Civil Aviation University of China, Tianjin, China
[6]Hunan Guo Tian Electronic Technology Co, Ltd, Changsha, China
[7]Chengdu CAIC Electronics Co, Ltd, Chengdu, China
[8]Taiyuan Aviation Instrument Co, Ltd, Taiyuan, China
[9]Wuhan Aviation Instruments Co, Ltd, Wuhan, China
*Correspondence: mengjie.song@bit.edu.cn
https://doi.org/10.1016/j.xcrp.2026.103543

SUMMARY

Ice detection technologies are essential for mitigating icing hazards in energy, transportation, and other fields in cold and humid environments. This review systematically summarizes the sensing principles, performance metrics, optimization strategies, and applications of ice detection technologies. Based on the physical properties of ice, sensing technologies are classified into acoustic, optical, thermal, electrical, and mechanical, and systematically compared for their capabilities in detecting icing characteristics, including ice type, thickness, and distribution. Optical and acoustic sensors achieve accuracies of about 0.1 mm within a 13 mm detection range, whereas electrical and mechanical sensors offer accuracies of 0.2–1.0 mm within a 20 mm range. Optimization strategies focusing on structures, materials, and algorithms are examined. Representative ice detection products and engineering applications are comprehensively analyzed. Finally, challenges and future directions for intelligent and multimodal ice detection are assessed, providing guidance for accurate icing monitoring and effective ice hazard mitigation.

INTRODUCTION

Ice formation is widespread in energy and power, aerospace transportation, and other fields, and ice accumulation on equipment surfaces often has adverse effects.[1–3] Wind power generation systems, as a typical renewable energy technology, experience increased equipment loads due to ice accumulation on turbine blades.[4,5] This phenomenon reduces power output and can even trigger widespread shutdown incidents, severely compromising the reliability of wind power generation and equipment safety.[6,7] Power transmission and communication lines may break due to ice accumulation, and signal towers toppled due to ice accumulation may even cause casualties.[8,9] In the aviation field, ice accretion on aircraft surfaces severely degrades aerodynamic performance and poses a critical threat to flight safety. In 2019, Kazakhstan's Bek Air Flight 2100 experienced a catastrophic loss of altitude shortly after takeoff due to severe ice accretion, resulting in a crash with 12–13 fatalities.[10] Dangerous accidents also occurred in transportation areas such as road transport and ocean transport due to icing.[11] The icing disaster in vessels and polar expeditions presents a triple coupling risk, sinking due to hidden fissures, instability of deck ice-loads, and sudden reduction of power due to micro-ice on the rotor, which poses a fatal threat to personnel safety and equipment reliability.[12–14] To curb the various hazards caused by ice formation, the development and application of anti-icing and de-icing technologies have become an urgent industry need. However, the practical effectiveness of existing technologies is constrained by the level of ice condition sensing, leading to challenges such as difficulty in determining optimal de-icing timing, low efficiency, and high energy consumption.

Accurate acquisition of ice thickness, distribution, and growth rates is essential for achieving efficient, precise, and energy-saving anti-icing and de-icing operations. Therefore, developing highly sensitive and precise real-time ice detection technology is the core prerequisite and fundamental basis for establishing a comprehensive anti-icing and de-icing technology system.

This is an open access article under the CC BY license (http://creativecommons.org/licenses/by/4.0/).

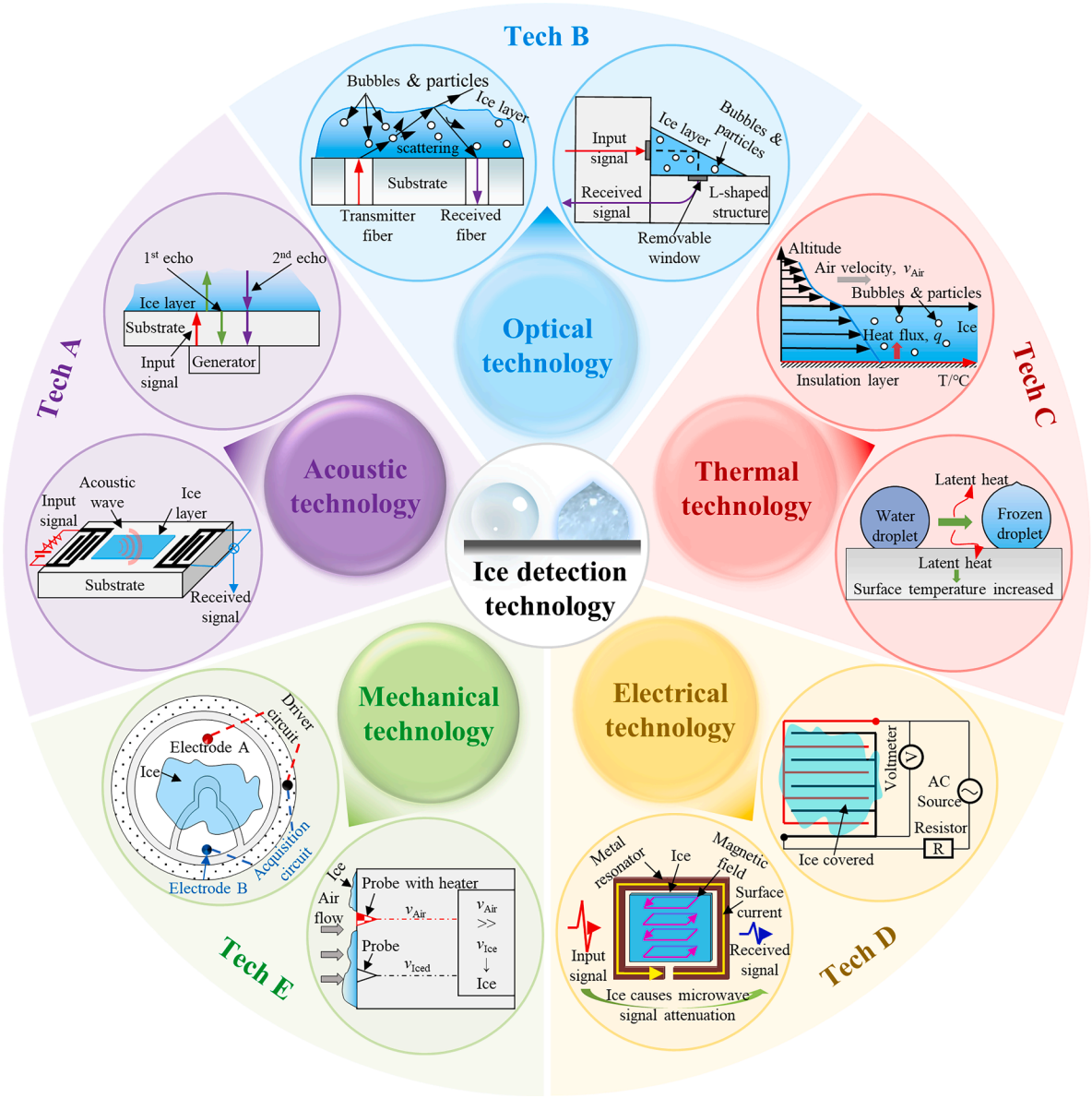

Figure 1. Ice detection technologies classification based on different physical characteristics

The essence of ice detection technology is to detect the properties of ice, which can be classified into five types from a physical perspective: acoustic, optical, thermal, electrical and mechanical,[15–17] as shown in Figure 1. A list of symbols and abbreviations is available in Table S1. In the acoustical region, the significant acoustic impedance difference between ice, water and air, as well as the reflection and refraction properties at the ice-substrate or ice-air interface, can be used to monitor the existence and thickness of ice.[18] The principle of ice detection based on the optical properties of ice is similar to that of acoustics. Ice detection can be determined by constructing a time-frequency character analysis on optical reflectance, scattering coefficient, or absorption coefficient of ice.[19] In the thermal region, the thermal conductivity of ice is about four times that of water, and its heat capacity is about half that of water. When water freezes into ice, it releases about 334 kJ/kg of latent heat of phase transition. Therefore, by monitoring the differences in these thermal properties to determine whether ice has formed, combined with thermal resistance and heat capacity analysis, it is also expected to achieve precise detection of ice thickness.[20] In the electrical region, there are significant differences in dielectric constant and electrical conductivity between ice and water at specific frequency bands. By combining time-frequency characteristics analysis, the type and thickness of ice can be determined.[21] In the mechanical region, ice adhesion causes changes in the mass and stiffness of the structure, which leads to a shift in its resonant frequency.[22] The existence of ice can be easily detected by monitoring the resonant frequency of the structure.

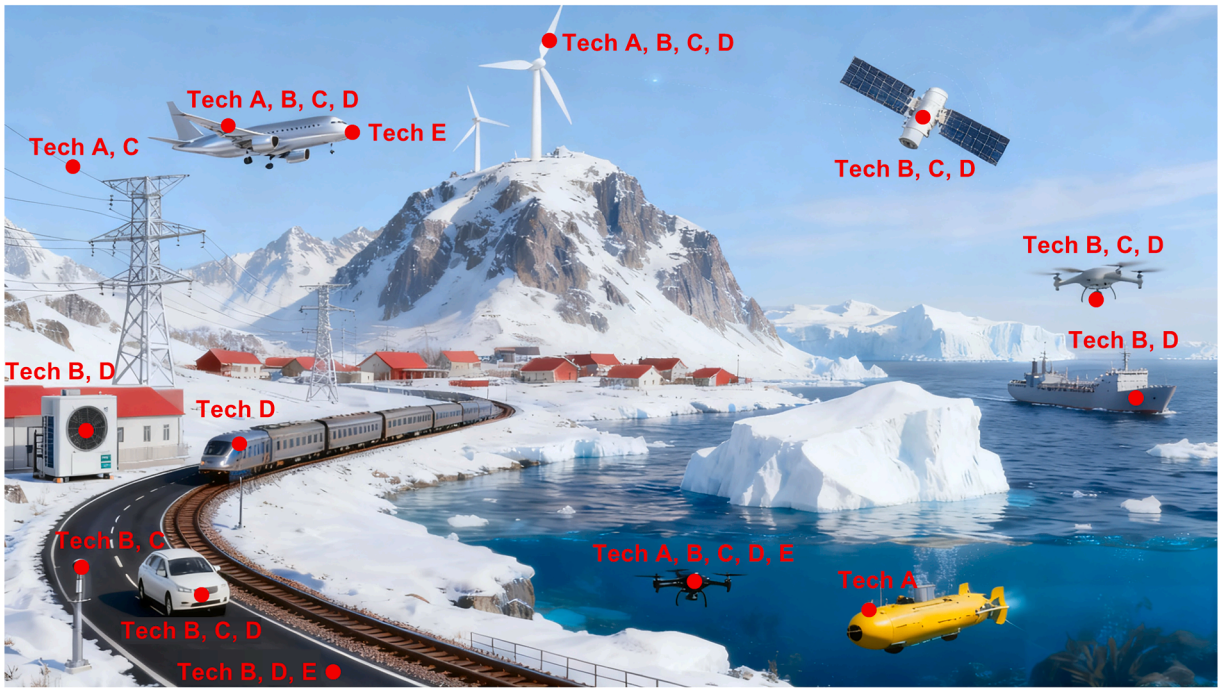

Figure 2. Applications of different types of ice detection sensors in various practical scenarios

In a word, precisely capturing and analyzing the changes in the physical properties of ice can significantly improve the accuracy of the ice detection sensor.

Over the past five decades, ice detection technology has undergone a transformative leap from point-based detection to area-based imaging detection, and subsequently to multi-modal intelligent systems.[23] Early aviation relied on single-point sensors such as mechanical resonant and differential pressure sensors, which only output Boolean values indicating the presence or absence of ice. Following the 1990s, breakthroughs were achieved in distributed detection technologies based on visible-infrared thermography and fiber-optic scattering sensors. Subsequently, after 2010, millimeter-level resolution surface icing imaging was progressively realized.[24] Over the past decade, multi-physics fusion methods such as capacitive tomography and ultrasonic guided waves have emerged. When combined with machine learning algorithms, they enable real-time detection of ice thickness, ice type, and even ice density under extreme conditions, including complex surfaces and turbulent boundary layers.[25–27] Moreover, the emergence of novel devices such as micro-thermal arrays, flexible electronic skin, and wireless passive surface acoustic wave (SAW) tags,[28–30] provides a foundation for optimizing ice detection sensors. Given the widespread occurrence of ice phenomena and detection requirements in diverse scenarios such as sky, land, and sea, the primary application scenarios for existing ice detection sensors of various types are illustrated in Figure 2.

Although several reviews have explored ice detection technologies, they are often confined to specific icing scenarios such as wind turbine blades and aircraft surfaces[4,16] or single sensing modalities such as thermal and infrared thermography applications.[31,32] To provide a more comprehensive perspective, this review establishes its novelty through three key additions. Specifically, this work discusses ice detection technologies across a broader range of scales, spanning from millimeter-level ice thickness on aircraft surfaces to meter-level sea ice. Furthermore, it deeply analyzes the underlying physical mechanisms of various sensing technologies alongside a comprehensive comparison of their performance parameters and an evaluation of specific practical ice sensor products. Moreover, the present review systematically summarizes optimization strategies for ice detectors, providing practical references for transitioning from laboratory concepts to engineering applications. Building upon this, this paper systematically summarizes the principles of existing ice detection technologies, categorizing various detection sensors based on five physical properties of ice: acoustic, optical, thermal, electrical, and mechanical. It quantitatively compares and analyzes the technical performance of each sensor type. Subsequently, we discuss research progress in optimizing ice detection sensors in terms of materials, algorithms, and other aspects. Finally, this work quantitatively compares the detection ranges and accuracies of existing ice detection sensors, summarizes their respective application scenarios alongside specific sensor products, and explores future development directions for intelligent ice sensors. This work aims to provide a valuable reference for researchers and engineering technicians in related fields.

ACOUSTIC ICE DETECTION SENSORS

The acoustic ice detection sensor works by monitoring the scattering and impedance effects of ice on the acoustic wave, which is shown in Figures 3A and 3B. The acoustic wave signal

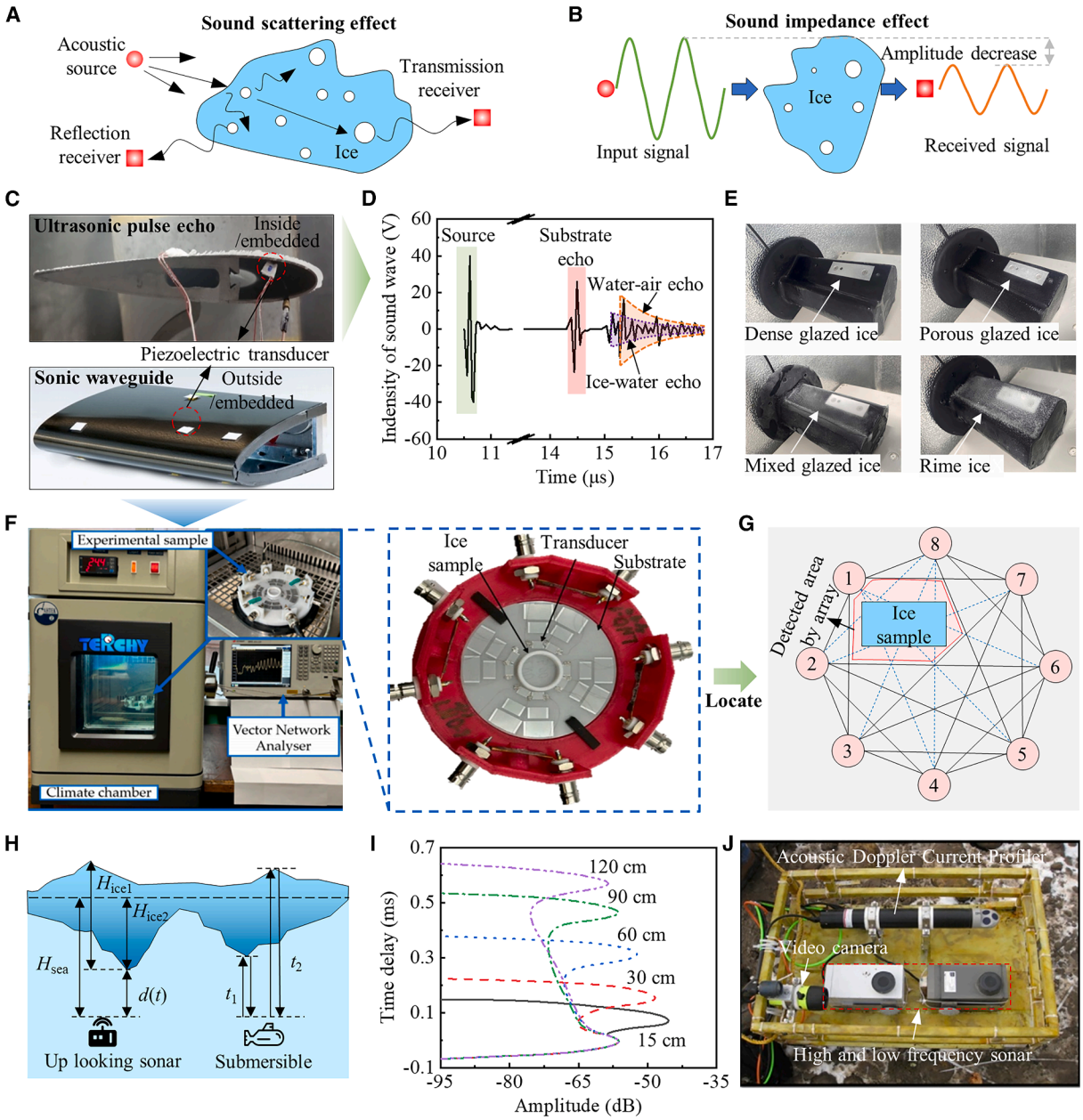

Figure 3. The principle, detection results, and devices of different acoustic ice detection sensors

(A) Schematic diagram of sound wave scattering effect when enter the ice body.

(B) Schematic diagram of sound wave impedance effect when enter the ice body.

(C) The installation positions of piezoelectric transducers under different detection methods. Adapted from Wang et al. under the CC BY 4.0 license, copyright 2022.[33]

(D) The ice-water interface detection result of ultrasonic pulse echo detection sensor.[34]

(E) Photos of the ultrasonic pulse echo ice detection sensor when detecting different types of ice. Reproduced from Ge et al. with permission from Elsevier, copyright 2025.[35]

(F) Ultrasonic waveguide ice detection sensor and experimental system for ice detection. Adapted from Smirnov et al. under the CC BY 4.0 license, copyright 2022.[36]

(G) The principle of ice positioning based on ultrasonic waveguide sensors array.

(H) Schematic diagram of the thickness detection of ice thickness detection sonar.

(I) Detection results of ice detection sonar at different ice thicknesses.[37]

(J) Device of high and low frequency ice detection sonar. Reproduced from Ghobrial et al. with permission from Elsevier, copyright 2013.[38]

will be scattered and attenuated as ice accumulates on the structure's surface. Researchers have applied a piezoelectric resonator on the icing surface to detect the influence of ice accumulation on acoustic wave parameters, such as the speed of sound wave propagation, the signal attenuation, and the frequency dispersion. As the piezoelectric resonator is applied inside the icing surface shown in Figure 3C,[33] the sonic pulse echo is dominantly focused, otherwise the wave signal attenuation is mainly analyzed.

The ultrasonic pulse echo (UPE) ice detection sensor monitors the time of delay (TOD) to calculate the ice thickness and analyze the ice type. The interface between ice and water film or between water film and air causes a significant echo pulse at different TOD,[34] as shown in Figure 3D. This method was already applied to underwater acoustic ice detection sensors in 1985, measuring ice thickness in the range of 1.5–31.0 mm with an absolute error of less than 0.5 mm.[39,40] Furthermore, researchers analyzed the attenuation of UPE to define the rime ice and clear ice. In this way, the UPE ice detection sensor has been optimized to be capable of accurately detecting ice thickness, and distinguishing ice types, even the roughness of the ice surface.[33,41] One of the influencing factors on the UPE ice detection sensor is the ultra-thin uneven water film on the ice top, which can lead to mistakes in ice top positioning. The micrometer-thick water film can hardly be removed and is too thin to be detected accurately. Some researchers have introduced multi-layer models into the UPE ice detection sensor, considering the physical properties near the ice-water interface as an interpolation of the physical properties of ice and water, which can achieve water film detection with a thickness resolution of 5 μm.[42,43] Many algorithms were introduced into the UPE ice detection sensor to optimize its detection results on multiple occasions, such as dynamic wavelet fingerprinting (DWFP) or neural network models.[44] After that, the water film on the ice top with a thickness of more than 30 μm can be detected and the ice type in Figure 3E can be distinguished with a classification accuracy of 87.8% as the ice growth and melting.[35]

The sonic waveguide ice detection sensors are usually designed as a circular array, as shown in Figure 3F, to detect the ice thickness and icing area.[36,45,46] The accumulated ice between two piezoelectric resonators leads to an attenuation on the sonic waveguide, as shown in Figure 3B. This sonic wave attenuation is directly influenced by the thickness and area of ice.[46] According to many experimental studies, the Lamb wave is regarded as one of the most suitable waveforms in sonic wave guide ice detection.[36] Its asymmetric mode is mainly influenced by liquid water, which is suitable for ice and water distinction, and its symmetric mode is suitable for ice thickness and area detection.[18] Furthermore, alongside Lamb wave-based sensors, SAW sensors have recently garnered significant attention. Due to their structural conformal coupling capabilities and ultra-high sensitivity to surface mass loading, SAW sensors exhibit unique advantages in micro-icing (early stage icing) detection. To elucidate the underlying physics, a theoretical SAW propagation model under icing conditions was constructed by Zhao et al.,[47] which systematically clarified the detection mechanism of SAW-based ice sensing. Building on this, the relationship between frequency shifts, temperature variations, and other key factors during the dynamic phase transition of water vapor was extensively investigated by Zeng et al.[45] using SAW devices, providing essential guidance for practical ice detection and monitoring. Remarkably, beyond highly sensitive micro-ice detection, the application of SAW technology has also been extended to active de-icing,[48] demonstrating immense potential for dual-functional icing protection.

The sonic waveguide ice detection sensors have been successfully applied on the multi-layer surface of aircraft or wind turbine blades, and can monitor ice accumulation that is more than 1 mm.[49,50] However, while ice thickness can be detected accurately when the ice area is fixed, it remains challenging to simultaneously decouple and clearly determine both the thickness and the area. Therefore, sonic waveguide ice detection sensors are extremely suitable for icing area detection, as shown in Figure 3G.[26] The attenuation of the sonic wave is significantly different depending on whether it is caused by ice or air. Therefore, the ice-influenced sonic waveguide between any two sensors in the array can be recognized, shown as a dotted line in Figure 3G, and the area of ice sampled can be clearly imaged.[27] Furthermore, by introducing classification and probabilistic models into sonic waveguide sensors applied to wind turbine blades, an ice presence detection accuracy of over 89.8% has been achieved within the monitoring area.[51,52]

The ice detection sonar operates by monitoring the time of flight (TOF) of acoustic pulse echoes. Unlike the UPEs ice detection sensor, the sonar does not contact with ice plate and is always underwater.[53] The principle of ice detection sonar is shown in Figure 3H, the ice thickness is calculated from the difference of TOF at the upper and lower surfaces of ice cover. The difference in TOF between the upper and lower surfaces of the ice plate increases with ice thickness, while the sonic wave amplitude changes inversely,[37] as shown in Figure 3I. The first submersible sonar applied to ice detection was installed on the Nautilus submarine in 1958, with a sea ice thickness detection absolute error of 2 m.[54,55] Some researchers also design mini submarines with ice detection sonar in the laboratory,[38] and test them in river ice detection as shown in Figure 3J. Furthermore, up-looking sonars fixed at the riverbed at depths of 100–150 m were capable of monitoring ice thickness over a long period, achieving an absolute error within the range of 5–30 cm.[56–59] No matter what kind of ice detection sonar, the sonic wave velocity in water and ice is the most important factor for its performance.[56,57] The wave velocity is about 3,700–3,900 m/s in sea ice, and about 1500 m/s in seawater.[37,60] It means that the milliseconds-scale error caused by pockets or cracks in ice will make an error more than 1 m in ice thickness detection.[61] By constructing an accurate ice body acoustic wave scattering model and combining it with wideband sweep technology, the thickness of sea ice with saltwater pockets or cracks can be detected with an accuracy of 1 cm in the laboratory.[38,62] However, achieving 1 cm accuracy with the real-world ice detection sonar is also extremely challenging.

Comparison of some acoustic ice detection sensors is shown in Table 1. By conformally coupling high-frequency sound waves with structures, ultrasonic echo and waveguide sensors achieve micro- to millimeter-level accuracy for thin ice ranging from 0.16 to 10 mm across varying localized detection areas. Conversely,

Table 1. Comparison on ice thickness and type detection performance of acoustic ice detection sensors

Item	Method	Embedded	Detection area	Thickness detection	Detection range	Detection accuracy	Ice type identification	Application	Year	Reference
A1	ultrasonic pulse echo	Y	3.1 cm^2	Y	0.3–10 mm	0.3 mm	N	aircraft	2025	Wang[63]
A2		Y	–	Y	0–1.55 mm	0.14 mm	N	aircraft	2022	Wang[33]
A3		Y	20.25 cm^2	Y	0–160 μm	8 μm	N	aircraft	2022	Wang[42]
A4		Y	–	Y	0–4.0 mm	0.1 mm	N	aircraft	2025	Zhang[34]
A5	acoustic waveguide	Y	–	Y	0–4.0 mm	0.2 mm	Y	wind turbine	2023	Zeng[45]
A6		Y	0–706.9 cm^2	N	–	–	N	aircraft	2016	Zhao[27]
A7		Y	0–100.0 cm^2	Y	0.5–1.5 mm	0.5 mm	N	aircraft	2024	Zhang[18]
A8	sonar	N	–	Y	0–10 m	~1 m	N	river navigation	2010	Marko[53]
A9		N	25.0 cm^2 1.0 m^2	Y	1.3–8 m	1 cm	N	polar navigation	2016	Lucieer[61]
A10		N	314.2 m^2	Y	0.15–0.9 m	~1 cm	N	polar navigation	2020	Bassett[37]
A11		N	4.0 m^2	Y	0.3–50 m	5 cm	N	polar navigation	2020	Khvorostovsky[60]

ice detection sonar systems cover large-scale areas, monitoring river channels or sea ice with centimeter-level accuracy over macroscopic ranges of 0.15–50 m, but they cannot detect millimeter-scale ice. Contact sensors sacrifice range for resolution, focusing on micro-scale ice warnings for aircraft wings and wind turbine blades. In contrast, contactless sensors sacrifice resolution for range, serving polar navigation and river ice mapping. Recent advancements in contact-echo ice thickness detection have demonstrated tailored performance based on target measurement ranges. Current sensors achieve an ultra-high accuracy of 8 μm for micro-scale icing within 160 μm, while maintaining reliable 0.1–0.3 mm accuracies within a 10 mm range for macroscopic ice layers. Meanwhile, the range of sonar ice thickness detection expanded from 10 to 50 m between 2010 and 2020, reflecting the parallel optimization of small-scale, high-precision and large-scale, wide-range technical routes. However, future cross-scale acoustic detection will primarily focus on stable ice type identification.

OPTICAL ICE DETECTION SENSORS

The optical ice detection sensor is working on the optical property of ice body, which is influenced by ice type and state. The visible and near-infrared refraction spectra of ice body from 0.2 to 1.2 μm is shown in Figures 4A and 4B. Different real and imaginary parts of refraction spectra between ice and water make it clear to distinguish the two materials. It is also fit to reflection spectra and scattering spectra,[64,65] and is the principle of optical ice detection sensor.

The optical fiber ice detection sensors are a typical ice detection device, and widely used in the detection of ice on the surfaces of aircraft, wind turbine blades, and transmission lines.[65,70] The ice thickness is calculated by measuring the TOF difference of the reflected light at the substrate-ice interface and the ice-air interface, and the ice type is identified by measuring the intensity of the reflected light.[71,72] Coaxial optical fiber ice sensor is one of the most typical structures. Its detection light intensity signal has a good linear relationship with ice thickness, but its detection sensitivity is relatively low.[70] It is often used for ice thickness detection below 5.0 mm, as shown in Figure 4D. By transforming the sensor detection into oblique fiber and wedge-shaped fiber, the ice thickness detection sensitivity of the sensor can be effectively improved, but the ice thickness detection range will be as low as less than 3.0 mm.[19,73] By paralleling one transmitting and six receiving optical fibers, the structurally simple sensor achieves ice thickness detection within the range of 0.7–1.5 mm under laboratory conditions.[74] In addition to structural optimization, integrating neural network algorithms with optical fiber sensors to analyze the relationship of ice thickness and ice type with relative received light intensity and TOF, yields an ice-type classification accuracy of 92.8% and an absolute error of 0.27 mm based on experimental tests.[75] Furthermore, a practical optical fiber sensor device was designed specifically to monitor real-time road surface states, ensuring transportation safety, as shown in Figure 4I.

The image identification ice detection sensor focuses on the visible reflection spectra of water and ice, it is usually applied to detect the icing state of cold surface.[76] By introducing some image recognition algorithms to the photos of light intensity, the icing area is easily recognized with higher accuracy.[77] However, moving people or vehicles will block the sensors recording photos of road surface, making them hard to be widely used in traffic.[68] One way to overcome this difficulty is applying the sensors on the vehicle, which is shown in Figure 4H, and this method for road state identification is still under investigation.[68,78] Furthermore, image recognition-based sensors can successfully identify river ice, achieving a relative area estimation error of less than 0.016% within a field of view of 0.4 km.[79] In addition, these sensors are capable of monitoring ice coverage in the polar regions with a theoretical classification accuracy of 96%.[80] On the other hand, the photo of icing edge on airfoil or wind turbine blade can be used to calculate the ice thickness by comparing

CellPress
OPEN ACCESS

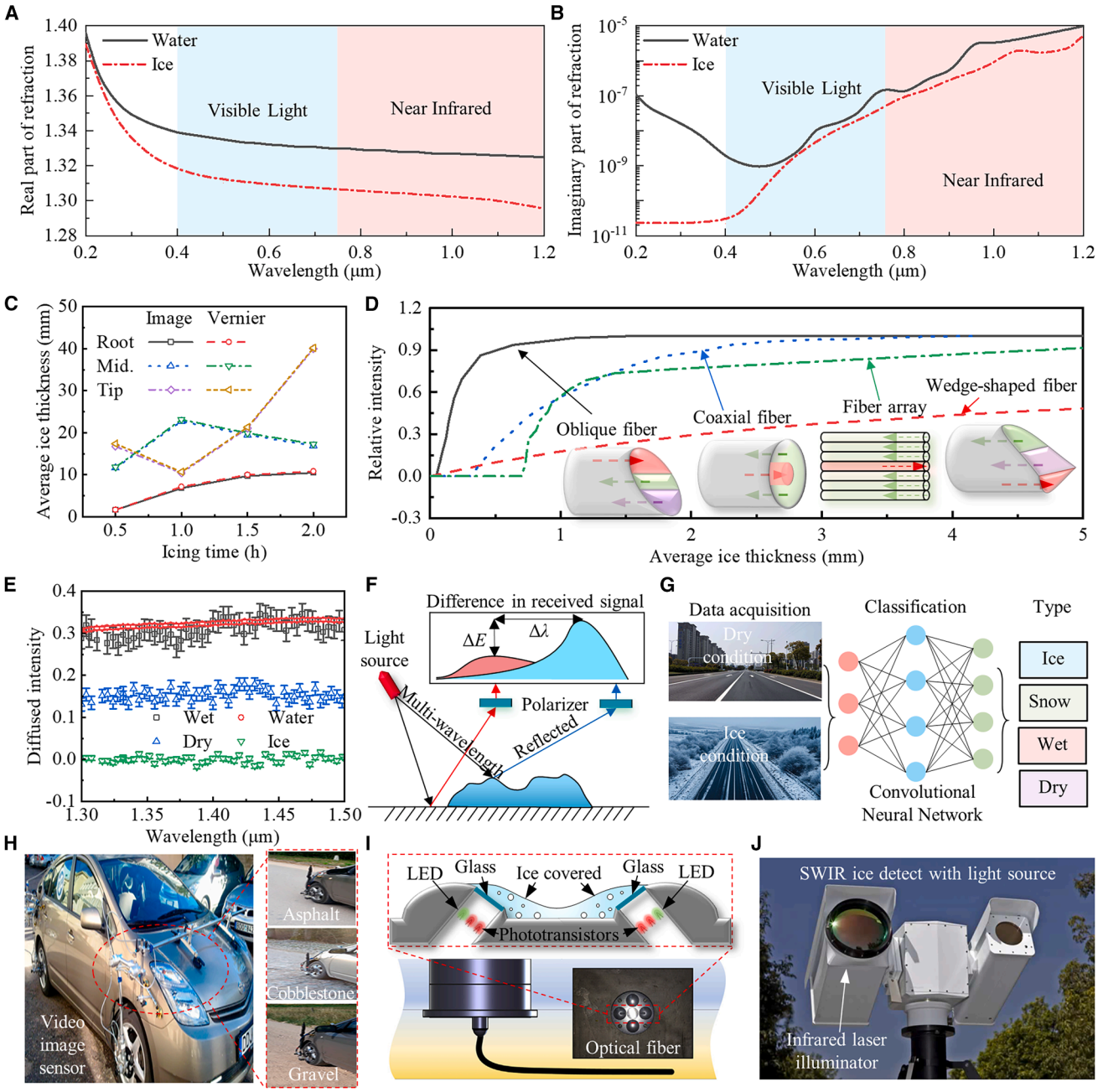

Figure 4. The principle, measurement results, and devices of optical ice detection sensors

(A) The visible and near-infrared refraction characteristic spectra of ice and water.

(B) The visible and near-infrared attenuation characteristic spectra of ice and water.

(C) Image processing results of ice detection on wind turbine blades.[66]

(D) Comparison of the performance of optical fiber ice detection sensors with different structures.

(E) Road surface condition detection results based on near-infrared polarized light. Error bars represent the standard deviation.[67]

(F) Schematic diagram of road surface condition detection based on near-infrared light.

(G) Optimization of road surface state classification based on neural networks.

(H) Vehicle-mounted road ice detection sensor based on image processing. Adapted from Šabanovi et al. under the CC BY 4.0 license, copyright 2020.[68]

(I) Fiber optic road ice detection sensor. Reproduced from Gui et al. with permission from Elsevier, copyright 2019.[17]

(J) Near-infrared polarized road surface condition detection sensor. Reproduced from Abdel-Moati et al. with permission from Elsevier, copyright 2018.[69]

Table 2. Comparison on ice thickness and type detection performance of optical ice detection sensors

No.	Method	Embedded	Detection area	Thickness detection	Detection range	Detection accuracy	Ice type identification	Application	Year	Reference
B1	optical fiber	Y	0.2 mm^2	Y	0–10 mm	~0.1 mm	Y	aircraft	2022	Ikiades[74]
B2		Y	21.3 mm^2	Y	0–3.5 mm	0.05 mm	Y	aircraft	2022	Ge[75]
B3	polarized light	N	0–0.1 km^2	N	–	–	N	polar navigation	2020	Buckley[89]
B4	image based	N	–	Y	0–40 cm	8.9 mm	N	wind turbine	2021	Hu[66]
B5		N	–	Y	0–13 mm	0.05 mm	N	line cable	2024	Dai[84]

with the original edge.[81,82] Some edge processing algorithms, such as Gaussian filtering, Laplacian edge enhancement, and the Canny edge detector, were introduced into these devices. At an observation distance of 0.5 m, the relative error for average edge ice thickness is as low as 2.62%,[66] as shown in Figure 4C. With extensive experimental and theoretical research, these sensors can measure ice thickness on thin cables with a relative accuracy of 90.6%, and the theoretical resolution of ice thickness detection is estimated at 0.05 mm.[83,84] In a word, the clear picture and excellent image identification algorithm is the dominating factor to ensure the performance of image identification ice detection sensors.

The principle of polarized light ice detection sensors is similar to image identification ice detection sensors. However, it focuses on the near-infrared spectra and the polarization method can reduce the adverse effect of ambient light on the ice detection results.[85] Therefore, photos of the frozen areas will be clearer and freely acquired without interference with less valid information. By extracting the texture information of the road surface from polarized images, the classification accuracy of road surface states can reach 92.3%,[67] as shown in Figures 4E and 4F. Even under nighttime conditions, polarized light ice detection sensors can maintain a road surface condition recognition accuracy exceeding 90%.[86] Some specific wavelengths, such as 0.94 or 1.65 μm, exhibit distinct absorption characteristics for ice and water, making them highly effective for phase differentiation. And the special wavelength illuminator enables the polarized light ice detection sensors to work even on foggy or rainy days.[87] By integrating neural network algorithms with multi-wavelength polarized icing sensors, the classification accuracy of road surface conditions can be further improved to over 95%.[17,88] A short-wave infrared (SWIR) ice detection sensor with an infrared laser illuminator was manufactured to work at night and autonomously detect ice on the road at long distances, as shown in Figure 4J.[69] However, these sensors could not detect the ice thickness and ice type on the road.

Comparison of some optical ice detection sensors is shown in Table 2, in which fiber optic ice detection sensors directly embedded into line cables or aircraft wing surfaces, achieving millimeter-accuracy of 0.05–0.25 mm in the 0–15 mm thickness range, and can effectively distinguish frost ice from glaze ice. In contrast, image-based and polarized ice detection sensors use non-contact optical imaging or TOF measurement to detect ice thickness with millimeter to meter accuracy within a macroscopic field of view of centimeters to hundreds of meters, effectively applied in polar navigation, glaciers and permafrost, and wind turbine blades, but still lack ice type identification capabilities at present. In the future, optical ice detection sensors will be optimized in three directions: high stability, full ice type identification, and sub-millimeter ice thickness detection, building a full-scenario, high-precision, and intelligent real-time ice detection sensor for aircraft, wind turbines, transmission lines, and polar navigation.

THERMAL ICE DETECTION SENSORS

Thermal ice detection sensors are based on the thermodynamic properties of ice. They identify ice and estimate its thickness by measuring the latent heat released during the ice formation process, changes in surface temperature, or differences in infrared radiation.[31] The latent heat ice detection sensor achieves ice detection by monitoring the rise in surface temperature when condensate water freezes to ice,[90] as shown in Figure 5A. Scholars have designed an ice detection sensor that monitors the temperature of cold surfaces through thermocouples and thermal resistance temperature sensors, and successfully detected a significant temperature rise on the cold surface at the moment of ice formation, as shown in Figure 5B.[91] Compared with being attached to the frozen surface, the temperature sensor array embedded in the frozen surface can detect the freezing moment more accurately,[91–93] as shown in Figure 5C. The volume of the frozen part directly determines the temperature rise of the frozen surface, but it is difficult to be quantitatively monitored. Therefore, the latent heat icing detection sensor can only detect the freezing moment currently. These sensors are usually used to detect the total water content (TWC), liquid water content (LWC), and ice water content (IWC) in atmosphere.[94] The Nevzorov cone is a typical latent heat ice detection sensor used to measure the TWC. When combined with a temperature sensor, it can predict icing conditions with a prediction accuracy of 80%–90%.[95] By optimizing the structural dimensions of the original Nevzorov cone, the relative accuracy of latent heat ice detection can be improved by over 7%.[96,97] Therefore, the Nevzorov cone is widely used in the detection of aircraft icing condition.

The sensible heat ice detection sensor is based on the change of thermal resistance and thermal capacity on the cold surface during ice accumulation, as shown in Figure 5D. The changed thermal capacity and resistance is calculated based on the changed temperature under heating supply and the thermal characters of ice, air, and cold surface.[99,100] The heating supply is usually from a film electric heater, and a film sensible heat ice detection device is shown in Figure 5E.[20] The volume of ice accumulation can be detected by sensible heat ice detection

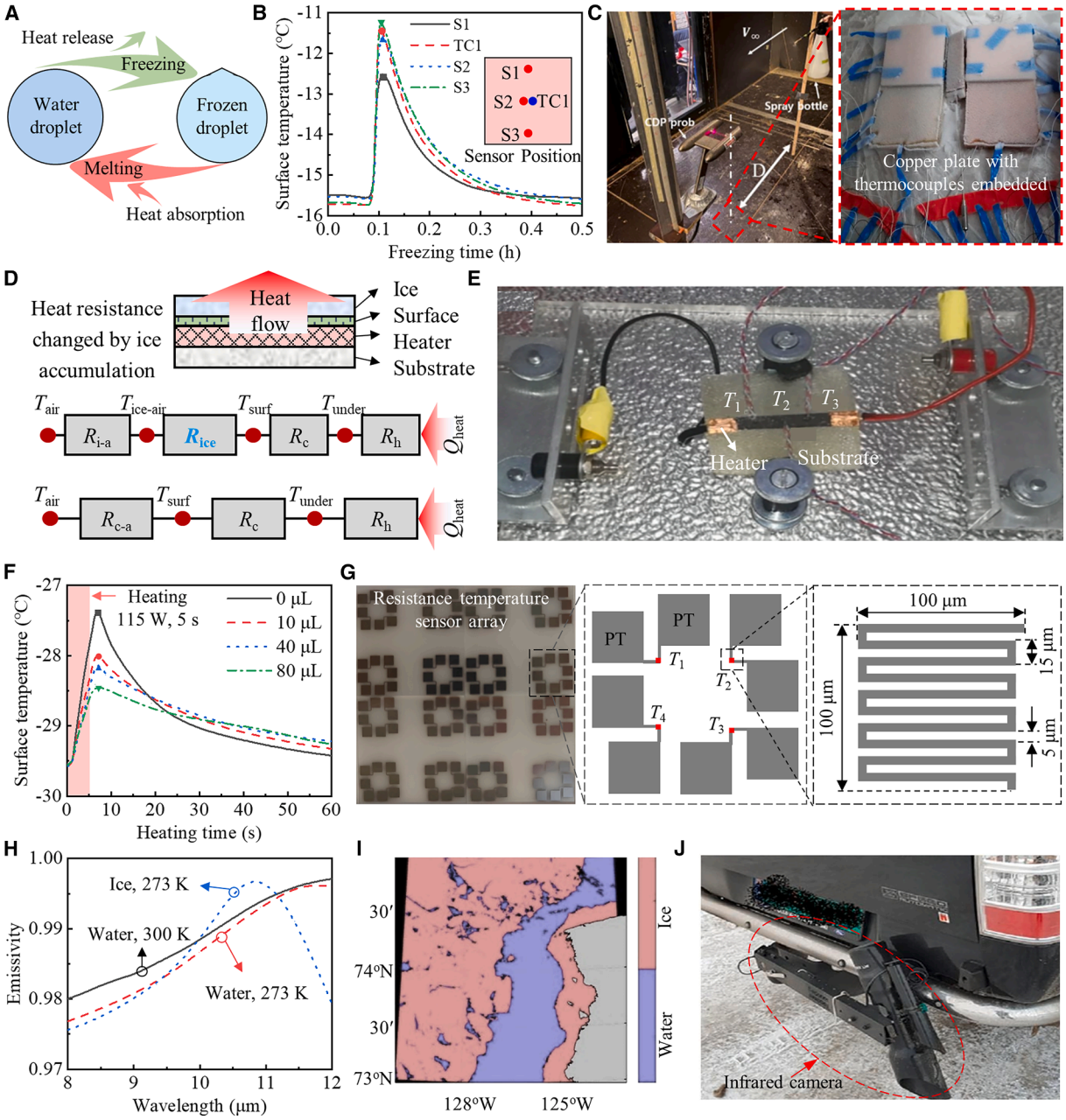

Figure 5. The principle, detection results, and devices of different thermal ice detection sensors

(A) The energy exchange when water transitions between different phases.

(B) The temperature rise caused by the freezing of condensate droplets.[91]

(C) Latent heat ice detection test system and copper plates embedded with thermocouples. Adapted from Rieman et al. under the CC BY 4.0 license, copyright 2020.[91]

(D) Schematic diagram of the principle of thermal pulse ice detection sensor.

(E) Thermal pulse ice detection device and system. Reproduced from Dongo et al. with permission from Elsevier, copyright 2021.[20]

(F) Detection results of thermal pulse ice detection sensor at different volumes of ice droplets.

(G) Platinum resistance temperature array ice detection sensor.

(H) The infrared emissivity of ice and water at different wavelength.

(I) The detection results of ice and water differentiation based on thermal infrared ice detection sensor. Reproduced from Ye et al. with permission from Elsevier, copyright 2024.[98]

(J) Vehicle-mounted infrared ice detection sensor. Reproduced from DiLorenzo et al. with permission from Elsevier, copyright 2023.[11]

Table 3. Comparison on ice thickness and type detection performance of thermal ice detection sensors

No.	Method	Embedded	Detection area	Thickness detection	Detection range	Detection accuracy	Ice type identification	Application	Year	Reference
C1	latent heat	Y	<1.0 mm^2	N	–	–	N	aircraft	2020	Rieman[91]
C2		Y	113.1 mm^2	N	0–14 mm	–	N	wind turbine	2022	Lucke[96]
C3	sensible heat	Y	<1.0 mm^2	Y	0–13 mm	~0.3 mm	N	wind turbine	2024	Zhang[100]
C4		Y	0–720.0 mm^2	N	–	–	N	glaciers and permafrost	2017	Tian[99]
C5	thermal infrared	N	163.4 cm^2	Y	0–20 mm	0.16 mm	N	aircraft	2022	Madi[113]
C6		Y	<1.0 mm^2	N	–	–	N	wind turbine	2016	Gómez[112]
C7		N	5,369.0 mm^2	Y	0–7 mm	<0.22 mm	N	traffic roads	2022	Li[115]

sensors in a fixed occasion shown in Figure 5F. The increased ice volume leads to a decrease in temperature rise under a fixed heating mode and air condition of −29.5°C. The pulse heating mode makes the temperature peak clearer, it is much easier to detect the ice volume in the range of 0–80 μL based on temperature rise under fixed pulse heating.[101] Besides the heating type, the type of the temperature sensors is also extremely important for sensible heat ice detection sensor. Its accuracy determines the performance of ice detection sensor. We have designed a heat pulse ice detection sensor with micro-nano structure thermal resistance temperature sensor array as shown in Figure 5G. The sensitive platinum resistance temperature sensor makes the ice detection results more accurate.

Except for the thermocouple and thermal resistance temperature sensors, the infrared thermal imaging sensors are also widely used to detect the icing area.[102] Its working principle is based on the different mid-infrared and far-infrared emissivity of ice and water at the same temperature, as shown in Figure 5H.[32] Due to the imaging errors caused by the inevitable inaccurate infrared temperature measurement, thermal infrared ice detection sensors are often used for large-scale ice area detection, such as sea ice distribution detection.[103,104] Therefore, the infrared spectrometers carried by many meteorological satellites, combined with the open water algorithm,[105] the normalized differential water index (NDWI) inversion algorithm,[106] or machine learning methods,[107,108] can achieve sea ice distribution detection with an area estimation error of less than 10%. The infrared imaging ice detection results near Banks Island are shown in Figure 5I.[98] By integrating multi-spectral imaging sensors covering visible to long-wave infrared bands, continuous acquisition of sea ice characteristics across a wide spectral range of 0.4–14.4 μm can be achieved.[107,109] In addition to the research on infrared detection sensors for large-scale sea ice distribution, some infrared icing detection sensors applied to aircraft,[110,111] wind turbine blades,[112] and transmission lines[99,113] have also been studied.[114] Infrared imaging is also used to identify the size of ice bodies. The minimum relative error in detecting ice thickness can be as low as 0.14%, and the minimum resolution of ice thickness can reach 0.1 mm.[113,115] Some thermal infrared ice detection sensors are also applied in vehicles to identify the icing conditions on road surfaces, as shown in Figure 5J, to ensure road traffic safety.[11,116]

Comparison of different thermal ice detection sensors is shown in Table 3. Sensible heat and latent heat ice detection sensors mainly use millimeter-scale chip embedding. Only sensible heat and thermal infrared imaging ice detection methods can identify ice thicknesses from 0 to 20 mm with the highest accuracy of 0.16 mm, and none of them have achieved ice type identification. The core challenges of thermal ice detection are the difficulty of simultaneously meeting the requirements of millisecond-level response and wide dynamic range. Furthermore, the significant temperature drift caused by complex environments, and the inability of a single thermal resistance model to distinguish ice types is also the disadvantage of thermal ice detection sensor. Therefore, future optimization of thermal ice detection sensors will primarily focus on achieving real-time detection and maintaining high stability.

ELECTRICAL ICE DETECTION SENSORS

Electrical ice detection sensors are based on the differences of electrical character between ice and water in terms of dielectric constant,[117–119] electrical conductivity,[21,120,121] as shown in Figures 6A and 6B. They convert the amount of ice accumulation into measurable electrical parameters or remote sensing changes in brightness temperature, achieving fast response, area or point ice identification.

As illustrated in Figure 6A, the complex permittivity, comprising the real part (ε') and imaginary part (ε''), exhibits distinct dielectric relaxation processes for ice and liquid water at 0°C. The dielectric relaxation of ice predominantly occurs in the lower frequency band around 10^4 Hz, whereas the relaxation of liquid water is distinctly observed in the microwave frequency band around 10^{10} Hz.[126] The capacitive ice detection sensor utilizes this principle to detect the size and type of ice through its capacitive structure. Four capacitive ice detection sensors with different electrode types are shown in Figure 6C. Concentric circular and rectangular electrode configurations are among the simplest capacitor structures and form the basis of capacitive ice detection sensors, providing an ice thickness measurement range of 0–5 mm.[127] A circular array capacitive ice detection sensor has been developed for the detection of ice on cylindrical surfaces such as transmission lines, which can detect an ice thickness of 10 mm.[128] Then, the interdigital structure, due to its high sensitivity, is one of the best-performing structures among the existing capacitive icing detection sensors.[129] The interdigital capacitance ice detection sensor can achieve an ice thickness detection error of less than 0.21 mm within the

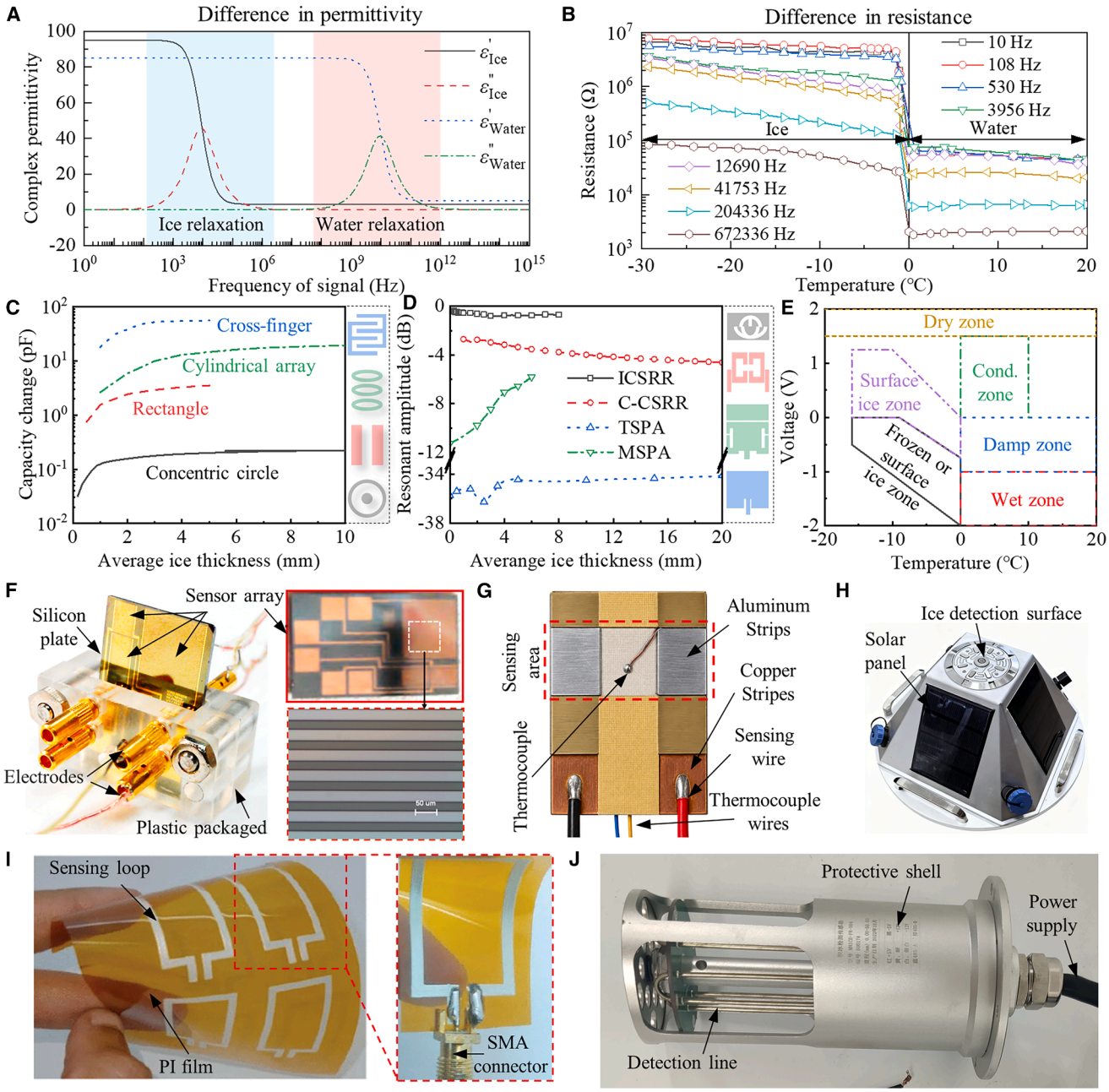

Figure 6. The principle, detection results, and devices of electrical ice detection sensors

(A) Distinct dielectric relaxation behaviors of ice and liquid water at 0°C.

(B) The resistance of ice and water at different frequency.[122]

(C) Comparison of capacitive ice detection sensors under different electrode structures.

(D) Comparison of microwave resonant ice detection sensors under different antenna structures.

(E) Phase diagram of the freezing state based on temperature and resistive ice detection sensor.[123]

(F) Interdigital capacitor array ice detection sensor. Adapted from Zhi et al. under the CC BY 4.0 license, copyright 2015.[124]

(G) Thin-film resistance ice detection sensor. Reproduced from Abdelaal et al. with permission from Elsevier, copyright 2022.[121]

(H) Solar-powered microwave ice detection sensor.

(I) Thin-film microwave resonant icing detection antenna. Adapted from Wagih et al. under the CC BY 4.0 license, copyright 2022.[125]

(J) Microwave ice detection sensor for power lines and cables.

Table 4. Performance comparison of electrical sensors for ice thickness and type detection

No.	Method	Embedded	Detection area	Thickness detection	Detection range	Detection accuracy	Ice type identification	Application	Year	Reference
D1	capacitive	Y	0–1350.0 mm^2	Y	0–8 mm	0.21 mm	N	aircraft	2025	Gui[25]
D2		Y	1500.0 mm^2	Y	1–4 mm	~0.2 mm	N	wind turbine	2024	Ur Rahman[127]
D3		Y	66.0 cm^2	Y	0–3 mm	0.2 mm	Y	aircraft	2022	Zheng[132]
D4	resistive	Y	108.0 mm^2	N	–	–	N	line cable	2022	Abdelaal[121]
D5		Y	–	Y	0–1.8 m	2 cm	N	river navigation	2015	Cui[15]
D6	planar microwave resonator	Y	25.0 mm^2	N	–	–	Y	aircraft	2019	Wiltshire[141]
D7		Y	136.5 mm^2	Y	0–20 mm	~0.3 mm	N	aircraft	2025	Shi[120]
D8		Y	450.0 mm^2	Y	0–6 mm	1 mm	N	radar cover	2021	Tariq[138]

range of 0–10 mm. By further coupling neural networks[130,131] and machine learning[124] to capacitive ice detection sensors, the detection accuracy of the sensor can be further improved, and its ice type identification capability can be expanded. When detecting ice accretions with a thickness of within 2 mm, the relative error for thickness is less than 10%, while the ice-type classification accuracy reaches 98.8%.[130,132] Therefore, some capacitive ice detection sensors have now been integrated and miniaturized as shown in the Figure 6F, and is widely used in aerospace, transportation, and other fields.[124,133] Furthermore, the capacitive ice detection sensor is able to detect the thickness of frost,[126,134] and even the interface position of ice-water mixture.[135,136]

Planar microwave resonance ice detection sensor also depends on the different permittivity of ice and water, but at the frequency around 10^{10} Hz shown in Figure 6A. Microwave resonant ice detection sensors with different structures exhibit varying ice thickness detection capabilities, as illustrated in the Figure 6D. The resonant frequency of the interdigital-complementary split-ring resonator (ICSRR) sensor is sensitive to variations in ice thickness, whereas the resonance amplitude remains largely unaffected by ice thickness changes, detecting only ice thicknesses within 8 mm.[137] The microstrip patch antenna (MSPA) sensor primarily perceives ice thickness variations within the 0–6 mm range through changes in the resonance amplitude, with its operating frequency exhibiting minimal variation in response to ice thickness change.[138] Although the T-shaped patch antenna (TSPA) sensor possesses a 20 mm detection range, its sensitivity is comparatively low.[139] A capacitively coupled split ring resonator (C-CSRR) sensor, which was innovatively designed by Song et al., exhibits a monotonic variation in its resonance amplitude within a 20 mm range, achieving a measurement range that far exceeds that of other planar microwave resonant ice detectors.[21,140] Although microwave resonant ice detectors as shown in Figures 6I and 6J can already measure ice thickness, research into algorithms for further enhancing its thickness detection accuracy remains immature.[125,141] These sensors are typically used to detect the frosting and icing processes, and are even capable of detecting the interface position between saltwater and marine ice within a range of 0–20 mm, achieving a relative measurement accuracy of 87.8%.[21,142] Neural network models have been introduced into microwave resonance ice detector, evaluating the accuracy of the icing state to be more than 93.33%.[143] However, the improvement of the ability of ice type identification of the microwave detection sensor is still under investigation.

The resistance of ice and water at different frequencies is extremely different as shown in Figure 6B.[122] Therefore, the resistive ice detection sensor can distinguish the solid or liquid phase as water freezing to ice. Due to the uncertainty of ice resistance at different temperatures, the resistive ice detection sensors can also detect the temperature of ice body to improve the accuracy of sensors.[121] The ice detection map based on the resistive ice detection sensors is shown in Figure 6E.[123] By arranging resistive ice detection sensors at equal intervals, it is even possible to measure the thickness of ice formations. Besides detecting the resistance of ice continuously, electrical resistivity tomography is widely used to detect water and ice in frozen soil.[144,145] By measuring resistivity distributions in frozen ground using transient electromagnetic field loading, ice and water distributions are distinguished based on their respective resistivity values.[146–148] The resistive ice detection sensor is usually designed as a film array structure as shown in Figure 6G.[121]

As shown by the parameters of electrical ice detection sensors in Table 4, it can be seen that capacitive, resistive, and microwave resonant ice detection sensors are all dominated by millimeter or centimeter-level embedded sensing, with detection areas ranging from 113.10 mm^2 to 50 cm^2, and can be embedded or attached to curved surfaces such as aircraft wing surfaces and wind turbine blades on line cables. Among them, the capacitive ice detection sensor has exhibited a maximum absolute error of 0.2 mm in the range of 0–9.1 mm. The core problem of electrical ice detection sensors is that the difference in dielectric constant between ice and water varies highly nonlinearly with temperature, salt content, and frequency, leading to errors in detection results. Improvement to the electrical ice detection sensor based on deep learning can effectively reduce the probability of misjudgment. In addition, high humidity, high salt spray, and vibration environments cause sharp changes in electrode polarization impedance, resulting in distorted detection results. Therefore, improving the robustness of electrical ice detection sensors will be the focus of its optimization.

MECHANICAL ICE DETECTION SENSORS

When ice accumulates on structures, the mass or the adhesion of ice will influence the structure's mechanical characteristics.

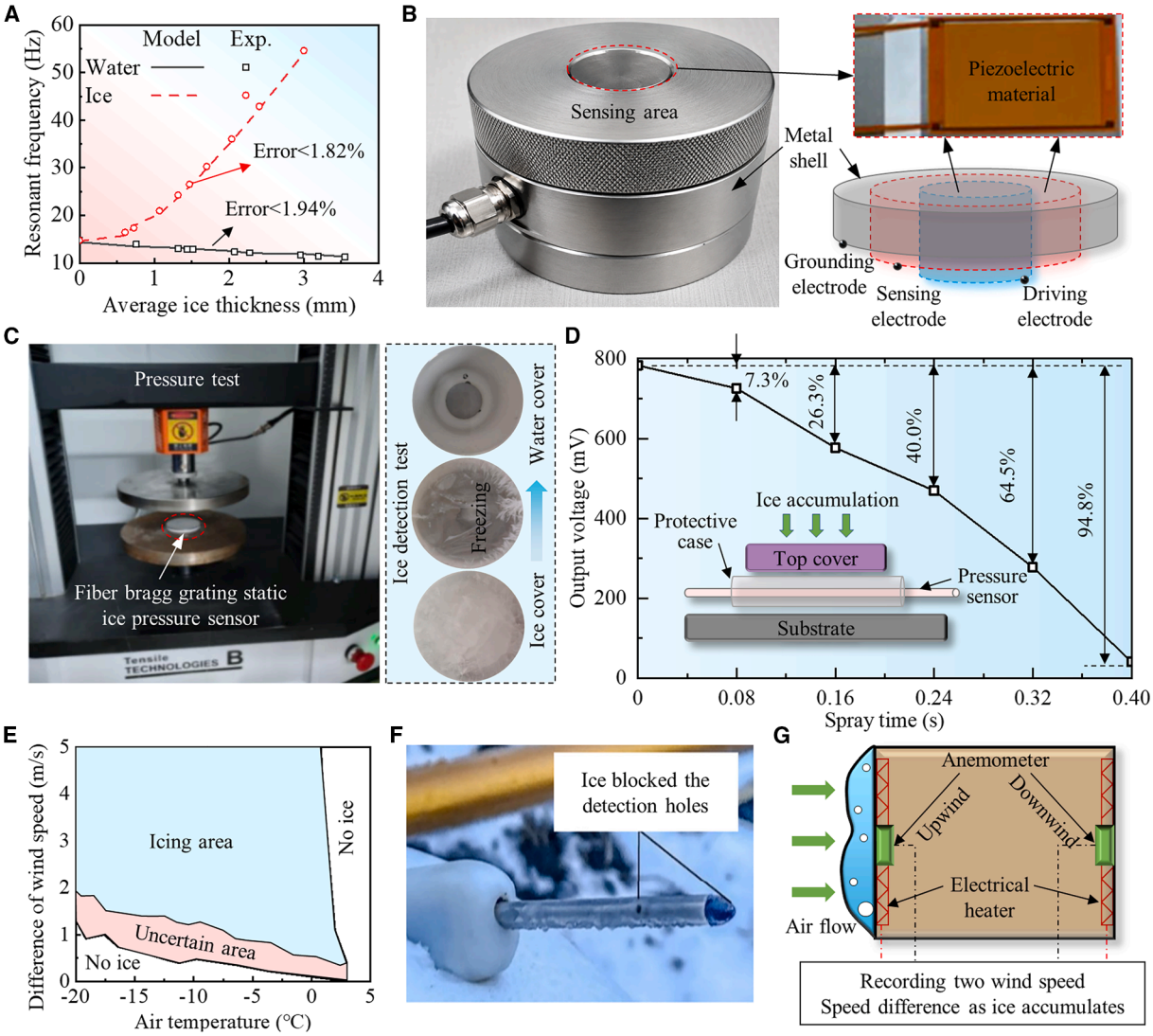

Figure 7. The principle, results, and devices of different mechanical ice detection sensors

(A) Ice thickness detection results based on piezoelectric resonance ice detection sensor.

(B) Structure of the piezoelectric resonant ice detection sensor. Reproduced from Gui et al. with permission from Elsevier, copyright 2019.[22]

(C) Pressure test and ice detection test of the strain gauge ice detection sensor. Reproduced from Zhang et al. with permission from Elsevier, copyright 2025.[153]

(D) Ice thickness detection results based on FBG strain-based ice detection sensor.[154]

(E) Wind turbine blade icing detection map based on dual wind ice detection sensor.[155]

(F) Dual wind speed ice detection sensor on aircraft. Reproduced from Han et al. with permission from Elsevier, copyright 2023.[151]

(G) Schematic diagram of the structure of the dual wind speed ice detection sensor.

Based on this, some mechanical ice detection sensors were designed and widely used to detect ice in aircraft, wind turbine blade, and so on. The stiffness and mass of the vibrating element change after icing, which leads to significant changes in its resonance parameters.[149] The essence of mechanical resonance ice detection sensors is to accurately measure the changes in resonance frequency to achieve efficient detection of icing conditions.[150,151] In addition, vibration de-icing can be achieved by the inverse piezoelectric effect of the vibration element, so the mechanical resonance ice detection sensor has an integrated function of ice detection and de-icing.[152] The ice thickness detection results of the piezoelectric resonance ice detection sensor and the sensor's physical diagram are shown in Figures 7A and 7B.[22] The relative error in ice thickness measurement between the sensor and the theoretical analysis is less than 1.94%. The piezoelectric material of the sensor is located in the central area and is protected by a metal shell, which can be embedded in the road ground for icing monitoring.

The strain-based ice detection sensor is essentially a deformation measurement device. When ice or snow accumulates on the sensor surface, the degree of deformation caused by pressure is monitored and the thickness of ice is calculated.

Table 5. Performance comparison of mechanical sensors for ice thickness detection

No.	Method	Embedded	Detection area	Thickness detection	Detection range	Detection accuracy	Ice type identification	Application	Year	Reference
E1	piezoelectric resonance	Y	505.8 mm^2	Y	0–10 mm	0.5 mm	Y	traffic road	2019	Gui[22]
E2		Y	–	Y	0–4.5 mm	0.1 mm	N	locomotive unit	2020	Zhao[157]
E3	strain gauge	Y	113.1 mm^2	Y	0–9.1 mm	~0.9 mm	N	bridge cables	2019	Zhang[131]
E4		Y	16.0 mm^2	Y	0–0.4 mm	0.1 mm	N	aircraft	2025	Zhang[153]
E5	dual wind speed	Y	–	N	–	–	–	wind turbine	2019	Swytink-Binnema[155]

Consequently, strain-based ice detection sensors require pressure testing and ice detection testing, as illustrated in Figure 7C.[153] Strain-based ice detection sensors utilizing piezoelectric crystals can detect ice thickness in the range of 0–9.12 mm, with a resolution of 0.91 mm.[131] The schematic structure and detection results of a fiber Bragg grating (FBG) strain-based ice detection sensor is illustrated in Figure 7D.[154] As ice layers progressively accumulate, the signal of this sensor monotonically decreases. Although strain-based ice detection sensors theoretically achieve ice thickness measurement, they cannot distinguish between ice, snow, and other contamination. Consequently, they have not gained widespread application.

The dual wind speed ice detection sensor determines the presence of ice by measuring the wind speed difference between the windward and leeward sides, as shown in Figures 7E–7G. The windward-facing hole may become obstructed due to ice accumulation, as illustrated in Figure 7G. The leeward-facing hole has a heater; when a wind speed differential exists, this indicates ice formation on the sensor surface.[156] The ice detection map based on dual wind speed ice detection sensor and ambient temperature sensor is shown in Figure 7E.[155] Should the hole of sensors become obstructed, the ice layer can be removed via electric heating to ensure continued sensing functionality. Given that the sensor detects only the presence of ice, it is typically installed on aircraft wings or wind turbine blades, as illustrated in Figure 7F, serving as an auxiliary detection tool.[151]

Comparison of different mechanical ice detection sensors is shown in Table 5. The common feature is that these sensors measure the mechanical character of ice or structure, such as resonant frequency drift or pressure difference, change as the ice accumulation, and the detection area is concentrated at 16.0–505.8 mm^2. Embedded installation can be achieved on traffic roads, or wind turbine blades. Specifically, mechanical resonance detection sensors exhibit an absolute measurement error ranging from 0.1 to 0.5 mm within the 0–10 mm range. However, most of the mechanical ice detection sensors cannot classify ice types clearly, but are widely applied on aircraft to ensure the safety of air transport.

OPTIMIZATION OF ICE DETECTION SENSORS

Performance optimization of icing detection sensors primarily focuses on three aspects: structural optimization, material optimization, and algorithm optimization. Fiber-optic, capacitive, and microwave ice detection sensors enhance their detection range or sensitivity primarily through structural optimization. The methods for optimizing the structures of these sensors have been compared and analyzed in the preceding sections.

Material optimization for ice detection sensors primarily focuses on acoustic, mechanical, and electrical ice detection sensors. Acoustic and mechanical ice detection sensors require piezoelectric materials to generate and capture mechanical vibration signal, analyzing vibration waveforms to determine the presence of ice. Optimizing piezoelectric materials is central to enhancing the performance of such sensors. The piezoelectric ceramic material was lapped to a thickness of 300 μm and then diced with a 20 μm wide groove. After injecting and filling epoxy resin, the material underwent grinding and polishing, followed by electrode sputtering on both upper and lower surfaces, as shown in Figure 8A.[63] An ultrasonic echo ice detection sensor constructed using these piezoelectric electrodes achieved a maximum absolute error below 0.29 mm in ice thickness measurement.[158]

The operational characteristics of electrical ice detection sensors are strongly correlated with the properties of their electrode materials. The electrical resistance of poly(3,4-ethylenedioxythiophene)-poly(styrenesulfonate) (PEDOT:PSS) hydrogels exhibits substantial variation between ice-covered and water-covered states, demonstrating excellent potential as an electrode material for ice detection sensors.[159] The structure of the PEDOT:PSS hydrogel in its dry state is shown in Figure 8B. As water covers the hydrogel, its internal electron transport pathways remain unchanged as shown in Figure 8C. However, when water within the hydrogel freezes and expands, it alters the distribution of PEDOT within the material, thereby impeding electron movement shown in Figures 8D and 8E.[161,162] Consequently, ice detectors constructed from PEDOT:PSS hydrogel exhibit enhanced capability to distinguish between ice and water phase.[163] Furthermore, graphene has been utilized as a conductive material in electrical ice detection sensors, as illustrated in Figures 8F and 8G.[160] Its negative temperature coefficient property, wherein resistivity progressively decreases with rising temperature, renders it suitable for application as a heating element for ice detection sensor based on the Joule effect. This enables ice detection at low currents and de-icing at higher currents, facilitating the construction of integrated detection and de-icing devices.

Data optimization methods may be applied to all ice detection sensors, particularly those based on waveform analysis and image processing. The operating principles of acoustic, optical,

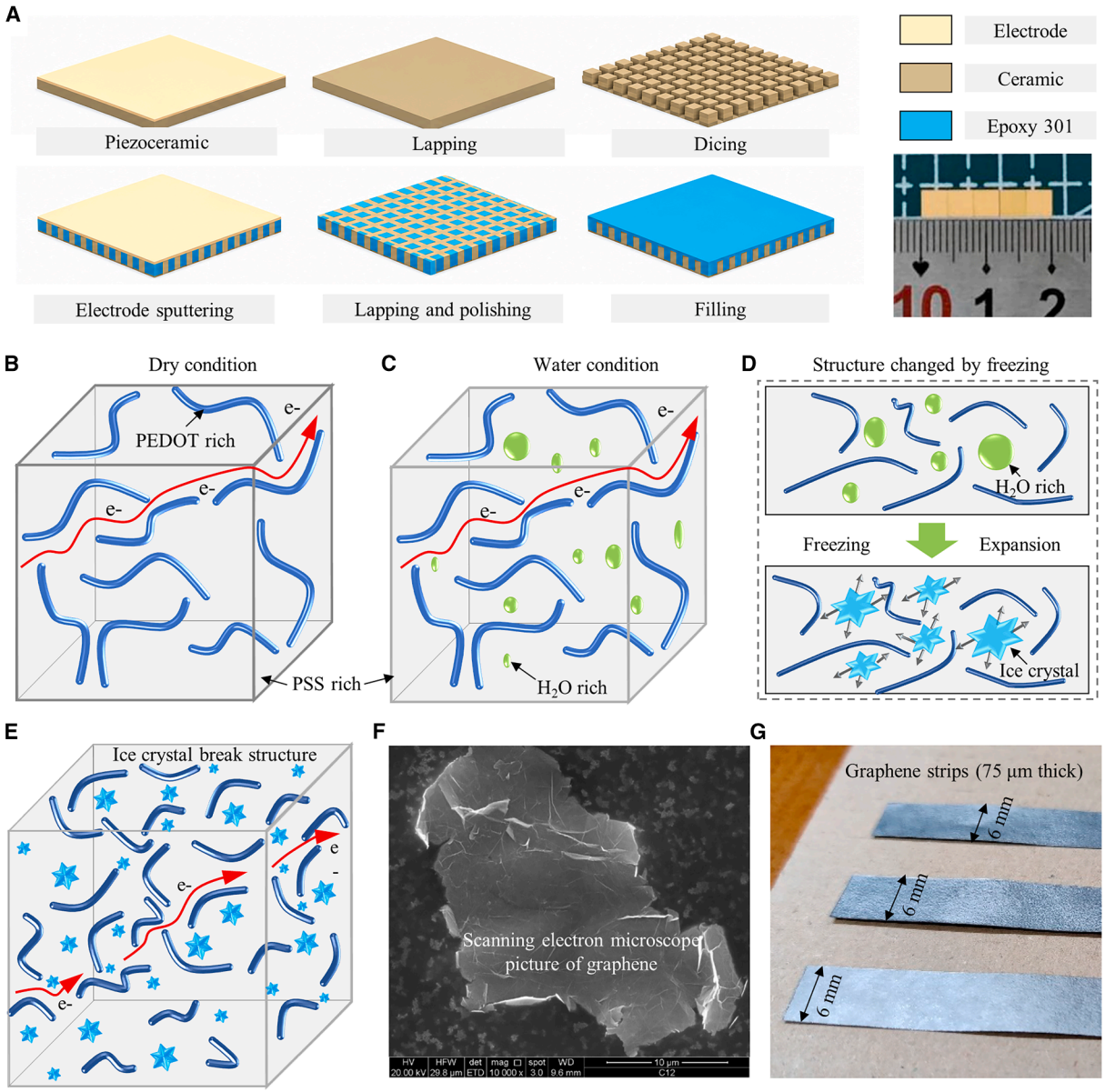

Figure 8. Optimization of materials on piezoelectric ceramics and electrodes for ice detection sensors

(A) Fabrication process for flexible, adhesive-coated piezoelectric ceramics.[63]

(B) Microstructural model of PEDOT:PSS hydrogel under dry conditions. Reproduced from Wang et al. with permission from Elsevier, copyright 2025.[159]

(C) Microstructural model of PEDOT:PSS hydrogel under water conditions.

(D) Structure change of PEDOT:PSS hydrogel as water freezing to ice.

(E) Microstructural model of PEDOT:PSS hydrogel under icing conditions.

(F) Scanning electron microscope picture of graphene.

(G) Graphene strips for capacitive icing sensor electrodes. Adapted from Sibilia et al. under the CC BY 4.0 license, copyright 2023.[160]

and electrical icing detection sensors all involve waveform analysis.[164] Consequently, data processing methods such as neural networks[34,131] and machine learning[35,130] are applied to these sensors. By employing principal component analysis (PCA) to extract waveform characteristics recorded by sensors under varying ice thicknesses, a principal component (PC) neural network model was constructed for ice thickness and ice type detection. These models shown in Figures 9A–9D were trained using extensive experimental data to achieve high-precision ice detection sensors.[165,166]

All ice detection sensors based on image data require optimization through image processing algorithms. Even sensors that detect ice via grey-scale extraction necessitate extensive experimental data to refine their discrimination thresholds for

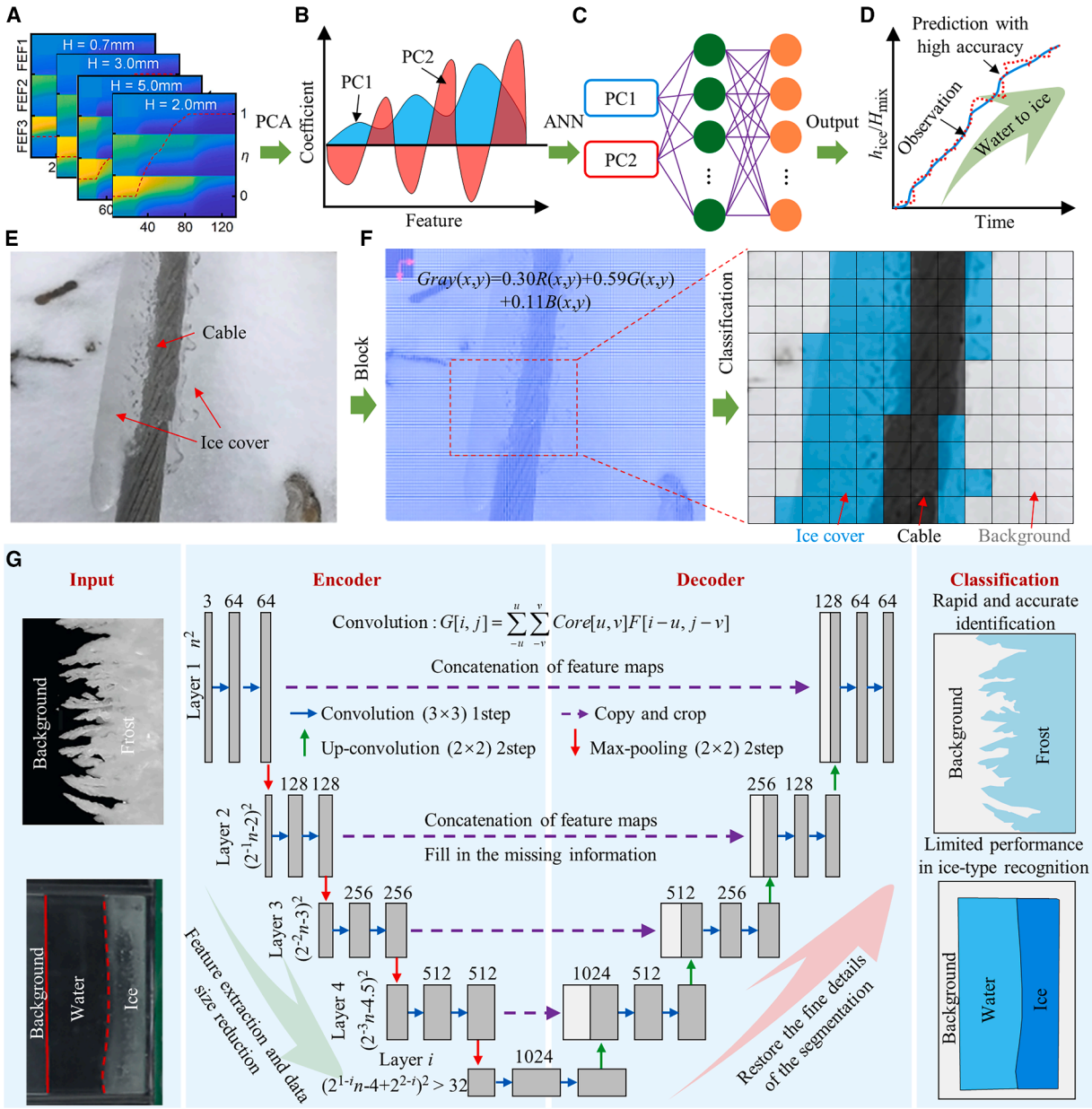

Figure 9. Algorithm optimization on signal and picture of the ice detection sensors

(A) Signal datasets recorded by electrical ice sensors at varying ice thicknesses.[166]

(B) Extracting waveform feature parameters based on principal component analysis.

(C) Construction of a neural network model for ice thickness detection.

(D) Validation of electrical icing detection sensor results based on neural network optimization.

(E) Original image of ice formation on steel cable surface. Adapted from Dai et al. under the CC BY 4.0 license, copyright 2024.[84]

(F) Ice-covered area distinction result based on grid partitioning and weighted average gray scaling.

(G) Ice formation image processing based on semantic segmentation methods.

identifying iced areas, as illustrated in Figures 9E and 9F.[84] Existing camera-based ice detection sensors typically convert captured images into gray scale using methods such as those illustrated in Figure 9F. The threshold for extracting iced areas within these gray scale images must be adjusted according to specific application scenarios. Furthermore, image segmentation methods based on convolutional neural networks (CNNs) represent the most widely applied approach in ice detection image processing.[66,76] Figure 9G illustrates a semantic segmentation approach based on a U-net CNN.[120,167,168] By applying successive layers of enhancement to captured images, the characteristic boundary lines between distinct regions within

the original image are accentuated. Subsequently, based on these feature boundaries and the enhanced data from the same layer, the image's fine details are restored.[169] By training on extensive datasets, the sensor's performance in rapidly and accurately identifying iced areas is enhanced. While the introduction of neural network algorithms improves the precision of iced area detection, it remains unable to effectively enhance the classification of icing types.

Beyond the aforementioned structural, material, and algorithmic optimizations, multimodal fusion has emerged as a crucial focal point for enhancing ice detection performance. Specifically, multimodal fusion encompasses, but is not limited to, the deep integration of multiple dimensions such as multi-sensor configurations, hybrid algorithms, and the systemic coupling of environmental and operational parameters. To illustrate these fusion paradigms, the significant potential of multimodal approaches has been demonstrated across various engineering applications. For instance, a complex impedance-based ice detection sensor was structurally optimized by He et al.[170] using an electrode array. By systemically coupling it with a temperature sensor, the temperature-induced variations in the dielectric constants of ice and liquid water were effectively compensated. Consequently, ice thickness detection on wind turbine blades within a 20 mm range was realized with a root-mean-square error (RMSE) of less than 1 mm. In the context of intelligent transportation systems, a multi-sensor fusion framework for black ice detection was developed by integrating image analysis, ambient temperature and humidity data, and acoustic signatures generated by tire-road interactions.[171] The "BlackIceNet" neural network model was constructed to analyze this fused data. After being trained with thousands of data samples, the model achieved a remarkable surface state classification accuracy of 97.54% during more than 200 validation tests. Furthermore, in the field of sea ice monitoring, a synergistic methodology capitalizing on the respective advantages of active and passive microwave remote sensing as well as optical remote sensing has been proposed by Huang et al.[172] Combined with deep learning algorithms, the simultaneous acquisition of macroscopic ice distribution and the precise extraction of sea ice geometric and surface features are facilitated by this cross-scale approach. Consequently, multimodal fusion not only breaks through the inherent performance bottlenecks of single-modal devices but also represents an inevitable technological evolution toward highly reliable, intelligent, and universally applicable ice detection systems.

In addition to technological advancements like multimodal fusion, establishing unified ice sample standards is equally critical for sensor refinement. Existing ice samples used for ice detection sensors are predominantly formed through ice wind tunnels or natural water freezing, yet no standardized ice sample specifications currently exist.[173,174] The frozen ice bodies produced under the ice wind tunnel test system can be used to simulate various types of aircraft surface icing, as illustrated in Figure 10A.[19,175,176] Numerous optical fibers, UPE, and microwave icing detection sensors installed on the airfoil model undergo testing within the ice wind tunnel for optimization.[158,176,177] Adjusting parameters such as supercooled large droplet (SLD) content, wind speed, and temperature within the ice wind tunnel simulates the variable operating environments of aircraft, enabling the production of different types of ice formations, such as glaze ice, rime ice, and mixed ice.[176,177] Calibrating various ice detection sensors using ice samples prepared under identical conditions in the ice wind tunnel enables the establishment of a unified comparative standard for aircraft and wind turbine blade surface ice detection sensors, thereby providing a reliable reference for optimization.

The formation of ice on road surfaces and rivers is a result of the natural freezing of water bodies. Consequently, verifying the capability of ice detection sensors is commonly achieved by either allowing natural freezing of water on the sensor or by placing prepared ice samples upon it. However, the distribution and content of air bubbles within ice formed from water freezing at different temperatures vary considerably,[1] which significantly affects the physical properties of ice bodies, such as optical refractive index or dielectric constant.[182,183] Therefore, constructing a standard clear ice body to evaluate the performance of various ice detection sensors under uniform conditions is crucial for assessing their performance. A stirrer was innovatively introduced by Song et al. to effectively dislodge bubbles from the ice-water interface, as illustrated in Figure 10B, thereby significantly increasing the existing clear ice preparation rate from approximately 3 to 8 μm/s.[178–180] Moreover, given that sea ice characteristically forms from the top downwards, a laboratory sea ice preparation system was designed by Song et al., as illustrated in Figure 10C.[181] By preparing a 3.5% salinity brine solution in the laboratory, they produced marine ice within this experimental system for the calibration of ice detection sensors. Furthermore, numerous researchers have developed similar apparatuses, and even designed brine ice tanks, thereby providing a support for the design and optimization of marine ice detection sensors.[184–186] In summary, although numerous ice detection sensors can measure ice thickness and ice type, the ice samples utilized by different researchers vary significantly, making it difficult to objectively compare the advantages and weaknesses of various sensors. Therefore, establishing a unified ice sample standard is crucial for optimizing ice detection sensors.

CONCLUSION AND OUTLOOK

The comparison of the ice thickness detection accuracy and detection range of different ice detection sensors is shown in Figure 11A. Most contact-based ice detection sensors have a detection range in 20.0 mm, with accuracy around 0.1–1.0 mm. The optical and acoustic ice detection sensors have a higher accuracy around 0.1 mm in the detection range of 0–13.0 mm. However, while these sensors exhibit high sensitivity, their performance degrades under environmental disturbances. In contrast, electrical and mechanical ice detection sensors maintain a stable measurement accuracy of 0.1–1.0 mm over a 0–20.0 mm detection range. These sensors can distinguish ice, water, and even pollution, and are widely used in aerospace, energy engineering, and so on. A special acoustic pulse echo ice detection sensor applied on an airfoil can even detect the μm-scale ice accumulation with an accuracy of 8.0 μm.[42] Additionally, an optical ice detection sensor is able to detect the ice thickness in the range of 0–13.0 mm with an accuracy of 0.05 mm. This sensor shows a good performance in mm-scale ice detection, which is suited to most icing occasions.

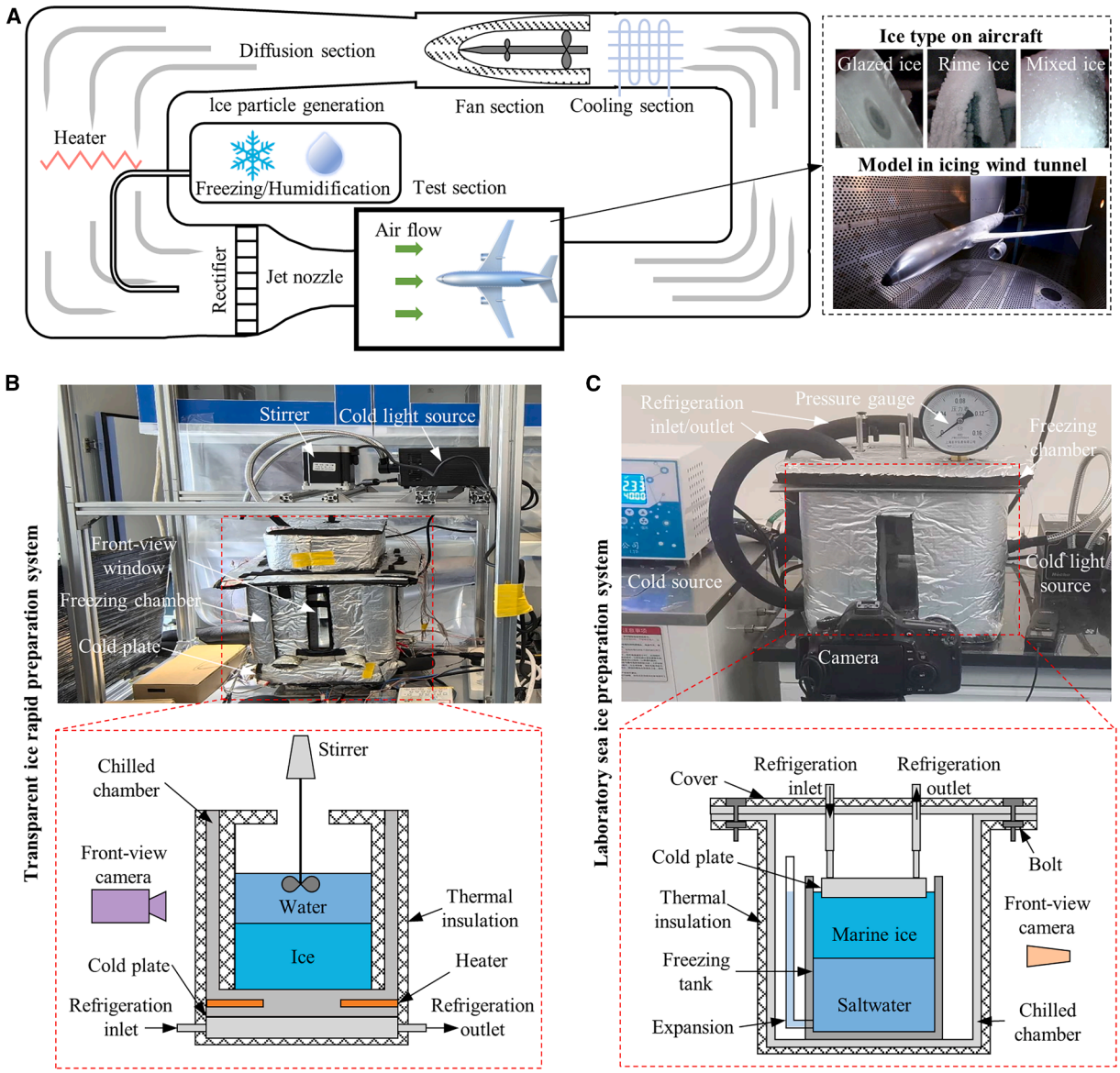

Figure 10. Complex ice preparation system for calibrating ice detection sensor

(A) Ice wind tunnel system for examining ice detection sensors on airfoil or wind turbine blades. Reproduced from Ge et al. with permission from Elsevier, copyright 2012.[19]

(B) A standard clear ice preparation system for calibrating ice detection sensors.[178–180]

(C) A laboratory system for preparing sea ice for calibration of ice detection sensors.[181]

For occasions that require the detection of sea ice, river ice, and road ice with contactless methods, remote ice sensors on unmanned aerial vehicles (UAVs) or satellites are widely applied. Comparison of some remote ice detection sensors on satellites is shown in Figure 11B and Table 6. The lidar and synthetic aperture radar (SAR) remote ice detection sensors are relatively accurate but with a narrower remote swath width under 10^3 km.[187,188] And most other microwave remote ice detection sensors have a coarser resolution with remote swath width around 10^3 km.[189,190] Therefore, the record database of the microwave remote ice detection sensor is much less than the lidar and SAR remote ice detection sensors. And the microwave remote ice detection sensors are suited to the wide polar ice detection under intricate weather. However, the lidar and SAR ice detection sensors are suited to detect ice areas on shipping lines or other meter-scale solutions requiring observation on sunny days. The detection resolution of visual identification system (VIS) or infrared spectroscopy (IR) remote sensing ice detection sensors lies between that of lidar remote sensing and microwave remote sensing. These VIS and IR remote ice detection sensors have limited resolution and cannot detect clearly at night or in foggy weather, but are relatively cheap

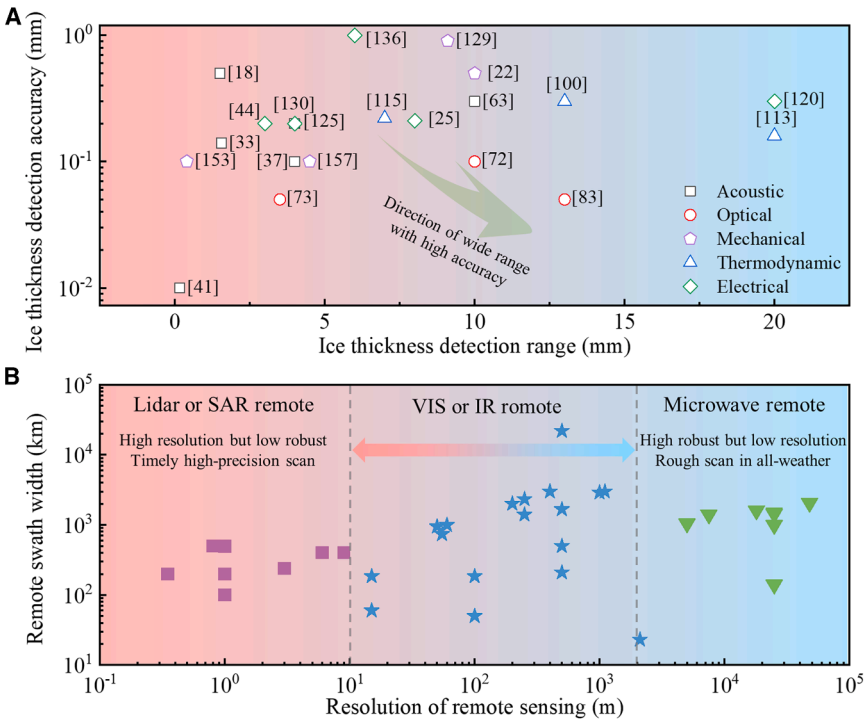

Figure 11. Comparison of contact icing detection sensors with remote sensing icing detection sensors

(A) Comparison of contact-based detection sensors for ice thickness detection.

(B) Comparison of remote sensing detection sensors for ice area detection.[187–190]

and easy to analyze the ice area. They are also widely used in remote ice detection.

Significant progress has been made in the application of icing detection sensors across the aerospace, power grid, and transportation (road and marine) sectors, with some systems already achieving commercial deployment, as illustrated in Figure 12.[16] For instance, certain mechanical resonance and fiber-optic sensors are currently deployed on aircraft to ensure operational safety. Additionally, microwave icing detection sensors designed for power transmission lines are now extensively utilized in Hubei Province, China. Road icing detection systems—integrating ground-embedded mechanical, microwave, and fiber-optic sensors with visual ice detection cameras—have also reached the field validation stage.[130,149] Meanwhile, meteorological satellites have long been equipped with lidar and microwave radar to monitor sea ice distribution.[191,192]

However, due to the diversity of icing scenarios, transitioning these icing detection sensors from laboratory research to broader field deployment remains challenging. Fundamentally, aerodynamic and structural compatibility poses a primary physical constraint, as protruding sensors on surfaces like aircraft wings and wind turbine blades can severely alter local airflow. To mitigate this aerodynamic penalty, many practical sensor designs are now mandated to be attached to the internal skin or embedded flush with the surface.[193,194] Beyond these physical limitations, environmental adaptability and lifespan are severely tested in field conditions, where extreme low temperatures, vibrations, and surface contamination such as dust and oil degrade long-term reliability. To counter this, integrating packaging materials with superhydrophobic or self-cleaning coatings has proven effective in mitigating surface contamination and corrosion.[195,196] Compounding these technical hurdles, a strict cost-performance trade-off limits large-scale deployment, as the prohibitive costs of high-precision sensors make extensive monitoring networks impractical. To address this dilemma, the rapid advancement of micro-electro-mechanical systems and printed flexible electronics is significantly reducing manufacturing costs, enabling broader distributed deployment.[25,139] Collectively, these targeted technological advancements are laying the essential groundwork for transitioning sensor devices from laboratory concepts to viable engineering tools.

In this review, we have systematically summarized the types and characteristics of icing detection sensor devices, alongside optimization strategies involving different sensor materials, algorithms, and sensor calibration. Regarding sensor types, acoustic and optical ice detection sensors are highly suitable for detecting ice layers or water films ranging from micrometers to millimeters in scale, achieving a maximum thickness resolution of 8 μm. This capability exactly fulfills the critical requirement for detecting 0.3 mm ice layers on aircraft surfaces. Notably, micro-scale bubbles within the ice and brine channels induce significant scattering and interference, which reduces thickness detection accuracy but simultaneously provides a quantifiable acoustic basis for ice type identification. Thermal icing detection sensors primarily serve icing environment monitoring but remain incapable of precisely identifying ice type, distribution, or thickness characteristics. Electrical and mechanical icing detection sensors consistently achieve an ice thickness detection accuracy of 0.1–0.3 mm. Wind tunnel experiments demonstrate their ability to resolve ice layers between 0.06 and 0.45 mm, and they are now widely deployed for icing monitoring on aircraft and roadways. Regarding sensor optimization, the detection sensitivity and thickness resolution of acoustic, mechanical, and electrical sensors can be significantly enhanced by optimizing piezoelectric or electrode materials. Furthermore, to overcome the inherent limitations of single ice detection devices, multimodal fusion has emerged as a crucial optimization strategy. By deeply integrating diverse physical mechanisms and multi-scale modalities, and synergizing these enriched hardware data streams with advanced computational algorithms, researchers can develop more universally applicable and robust systems capable of self-learning, self-calibration, and autonomous decision-making. Additionally, establishing a comprehensive data platform and standardizing ice type and thickness measurements would facilitate fair comparative evaluations under identical conditions, thereby delineating the optimal

Table 6. Types and operating parameters of remote ice detection sensors

No.	Remote type	Sensor type	Satellites	Resolution (m)	Swath width (km)
1	VIS or IR	AHI	Himawari-8/9	500	500
2	VIS or IR	AMI	GEO-KOMP-SAT-2A	500	22,000
3	VIS or IR	ASTER	Terra	15	60
4	VIS or IR	AVHRR/3	NOAA-18	1,100	3,000
5	VIS or IR	AVHRR/3	Metop-B	1,100	3,000
6	VIS or IR	AWiFS	RE-SOURCE-SAT-2	55	740
7	VIS or IR	CZI	HY-1C/1D	50	950
8	VIS or IR	FCI	MTG-I1	500	210
9	VIS or IR	I-2	HJ-2A/2B	100	50
10	VIS or IR	KMSS	Meteor-MN2-2	60	1,000
11	VIS or IR	MODIS	Terra	250	2,330
12	VIS or IR	MSU-MR	Meteor-MN2	1,000	2,900
13	VIS or IR	MSU-MR	Meteor-MN2-2	1,000	2,900
14	VIS or IR	MSU-IK-SR	Kanopus-V-IR N2	200	2,000
15	VIS or IR	OLI	Landsat-8	15	185
16	VIS or IR	OLI-2	Landsat-9	15	185
17	VIS or IR	PSS	Kanopus-V N5/N6	2,100	23
18	VIS or IR	SGLI	GCOM-C	250	1,400
19	VIS or IR	SLSTR	Sentinel-3A	500	1,675
20	VIS or IR	TIRS	Landsat-8	100	185
21	VIS or IR	TIRS-2	Landsat-9	100	185
22	VIS or IR	VIIRS	JPSS-1/2, Suomi NPP	400	3,000
23	SAR	PALSAR-2	ALOS-2	1	490
24	SAR	SAR 2000	COSMO-SkyMed 1	1	200
25	SAR	SAR	CSG-1	0.35	200
26	SAR	SAR	GF-3	1	500
27	SAR	SAR	NovaSAR-1	6	400
28	SAR	SAR-RCM	RCM-1/2/3	1	500
29	SAR	SAR	RADARSAT-2	0.8	500
30	SAR	SAR	RISAT-1A	3	240
31	SAR	SAR	Sentinel-1A	9	400
32	SAR	SAR	TerraSAR-X	1	100
33	Microwave	AMSR2	GCOM-W	5,000	1,045
34	Microwave	AMSU-A	Aqua	48,000	2,054
35	Microwave	ASCAT	Metop-B/C	25,000	1,000
36	Microwave	Radiometer	HY-2B	18,000	1,600
37	Microwave	Scatterometer	HY-2B	25,000	1,500
38	Microwave	Scatterometer	CFOSAT	25,000	1,000
39	Microwave	MWRI	FY-3C/3D	7,500	1,400
40	Microwave	OSCAT-3	Oceansat-3	25,000	1,440
41	Microwave	SWIM	CFOSAT	25,000	140

use cases for various sensor types. Ultimately, the systematic summary presented in this review is expected to serve as a valuable reference for transitioning ice detection technologies into practical sensor applications. As these integrated sensing technologies continue to mature, they will provide reliable technical support for ensuring aviation safety, improving wind energy utilization, and maintaining the stable operation of public infrastructure under freezing conditions.

ACKNOWLEDGMENTS

This research is funded by the National Natural Science Foundation of China (grant nos. 52576006, 52406007, and 52306003), the Beijing Natural Science Foundation (grant no. QG26007), the Beijing Municipal Commission of Science and Technology, Zhongguancun Science and Technology Park Management Committee (grant no. Z231100006123010), and the Department of Science and Technology of Hebei Province (grant nos. 244A7625D and 254Z4504G).

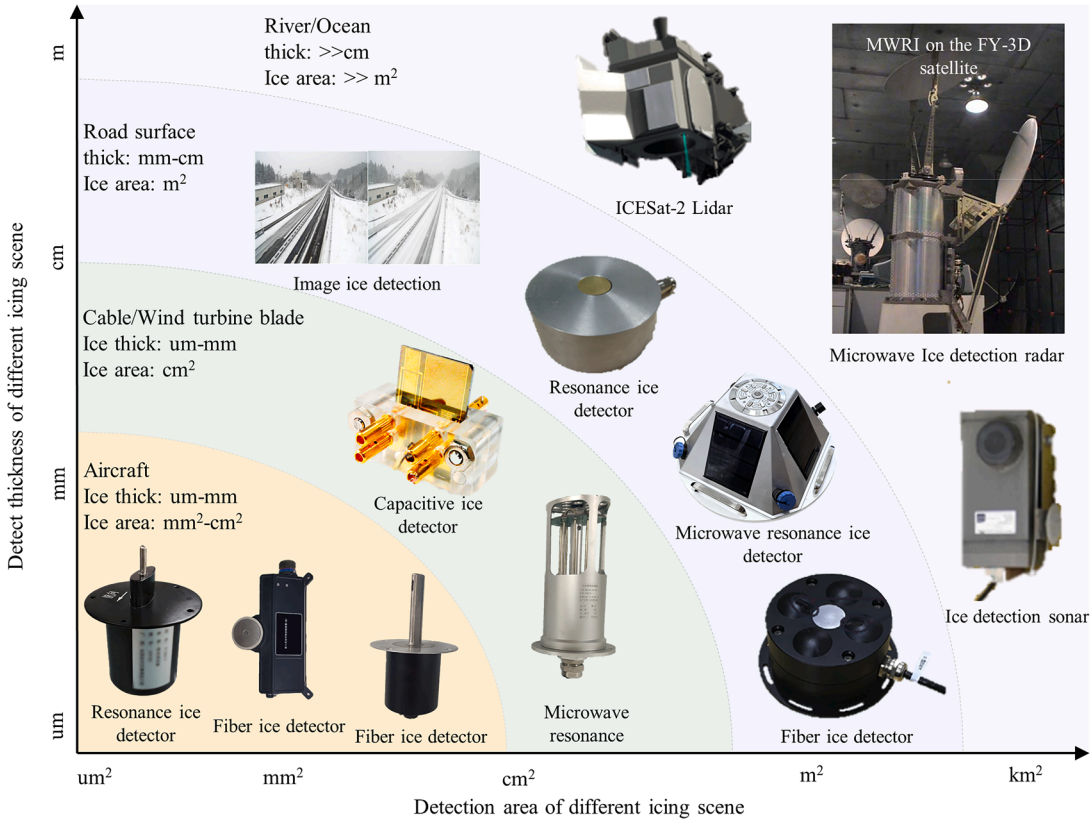

Figure 12. Various icing detection applications are supported by ice detection sensors

AUTHOR CONTRIBUTIONS

H.S., conceptualization, methodology, investigation, and writing – original draft; M.S., conceptualization, methodology, and writing – review and editing; X.Z., investigation and writing – review and editing; L.Z., investigation and writing – review and editing; K.S., visualization and writing – review and editing; Z.Z., data curation and writing – review and editing; R.G., visualization and writing – review and editing; C.Y.H.C., writing – review and editing; D.R.K., writing – review and editing; X.Y., investigation and writing – review and editing; B.C., writing – review and editing; B.H., investigation and writing – review and editing; Y.Z., investigation and writing – review and editing; Z.D., investigation and writing – review and editing; Z.X., investigation and writing – review and editing.

DECLARATION OF INTERESTS

The authors declare no competing interests.

SUPPLEMENTAL INFORMATION

Supplemental information can be found online at https://doi.org/10.1016/j.xcrp.2026.103543.

REFERENCES

1. Shao, K., Song, M., Shen, J., Zhang, X., and Pekař, L. (2024). Experimental study on the distribution and growth characteristics of trapped air bubbles in ice slices at different freezing temperatures. Appl. Therm. Eng. *244*, 122600. https://doi.org/10.1016/j.applthermaleng.2024.122600.
2. Liu, Z., Zhang, X., Song, M., Zhang, L., Shao, K., Zhen, Z., Liu, X., and Kim, D.R. (2024). Experimental study on heat transfer characteristics of ice melting processes under point-source bubble flows. Int. Commun. Heat Mass Transf. *159*, 108112. https://doi.org/10.1016/j.icheatmasstransfer.2024.108112.
3. Shao, K., Zhang, X., Song, M., Shen, J., Huang, L., Zhan, T., Wang, H., You, B., Pekař, L., Kim, D.R., et al. (2025). Manipulating trapped air bubbles in ice for message storage in cold regions. Cell Rep. Phys. Sci. *6*, 102622. https://doi.org/10.1016/j.xcrp.2025.102622.
4. Madi, E., Pope, K., Huang, W., and Iqbal, T. (2019). A review of integrating ice detection and mitigation for wind turbine blades. Renew. Sustain. Energy Rev. *103*, 269–281. https://doi.org/10.1016/j.rser.2018.12.019.
5. Guo, P., and Infield, D. (2021). Wind turbine blade icing detection with multi-model collaborative monitoring method. Renew. Energy *179*, 1098–1105. https://doi.org/10.1016/j.renene.2021.07.120.
6. Mu, Z., Guo, W., Li, Y., and Tagawa, K. (2023). Wind tunnel test of ice accretion on blade airfoil for wind turbine under offshore atmospheric condition. Renew. Energy *209*, 42–52. https://doi.org/10.1016/j.renene.2023.03.126.
7. Chuang, Z., Li, C., Liu, S., Li, X., Li, Z., and Zhou, L. (2022). Numerical analysis of blade icing influence on the dynamic response of an integrated offshore wind turbine. Ocean. Eng. *257*, 111593. https://doi.org/10.1016/j.oceaneng.2022.111593.
8. Rossi, A., Jubayer, C., Koss, H., Arriaga, D., and Hangan, H. (2020). Combined effects of wind and atmospheric icing on overhead transmission lines. J. Wind Eng. Ind. Aerod. *204*, 104271. https://doi.org/10.1016/j.jweia.2020.104271.
9. Chen, Y., Cai, Y., Xie, Q., Wan, J., and Sun, Q. (2024). Combined effects of icing and wind on transmission lines in mountainous areas. J. Constr. Steel Res. *223*, 109042. https://doi.org/10.1016/j.jcsr.2024.109042.

10. Aviation Safety Network (ASN) (2019). Accident Description: Bek Air Flight 2100, Fokker 100 UP-F1007 (Almaty. (Flight Safety Foundation)). https://aviation-safety.net/database/record.php?id=20191227-0.

11. DiLorenzo, T., and Yu, X. (2023). Use of ice detection sensors for improving winter road safety. Accid. Anal. Prev. *191*, 107197. https://doi.org/10.1016/j.aap.2023.107197.

12. Samuelsen, E.M. (2018). Ship-icing prediction methods applied in operational weather forecasting. Q. J. R. Meteorol. Soc. *144*, 13–33. https://doi.org/10.1002/qj.3174.

13. Huang, R., Zhang, X., Zhang, L., Gao, Y., Zhang, H., and Song, M. (2026). Icing characteristics of micropillar-encapsulated sessile water droplets on cold surfaces. Int. J. Heat Mass Transf. *261*, 128527. https://doi.org/10.1016/j.ijheatmasstransfer.2026.128527.

14. Müller, N.C., Løw-Hansen, B., Borup, K.T., and Hann, R. (2023). UAV icing: Development of an ice protection system for the propeller of a small UAV. Cold Reg. Sci. Technol. *213*, 103938. https://doi.org/10.1016/j.coldregions.2023.103938.

15. Cui, L., Qin, J., and Deng, X. (2015). Freshwater ice thickness apparatus based on differences in electrical resistance and temperature. Cold Reg. Sci. Technol. *119*, 37–46. https://doi.org/10.1016/j.coldregions.2015.07.009.

16. Maio, L., Moore, J., Cook, D.E., Potluri, P., and Bosetti, C.K. (2026). A review of ice detection technologies. Prog. Aero. Sci. *161*, 101158. https://doi.org/10.1016/j.paerosci.2025.101158.

17. Gui, K., Ye, L., Ge, J., Cheikh, F.A., and Huang, L. (2019). Road surface condition detection utilizing resonance frequency and optical technologies. Sensor Actuator Phys. *297*, 111540. https://doi.org/10.1016/j.sna.2019.111540.

18. Zhang, Y., Zhang, H., Yi, X., Wu, B., Guan, X., and Xiong, J. (2024). Analysis method and experimental study of ice accumulation detection signal based on Lamb waves. Chin. J. Aeronaut. *37*, 388–403. https://doi.org/10.1016/j.cja.2024.04.014.

19. Ge, J., Ye, L., and Zou, J. (2012). A novel fiber-optic ice sensor capable of identifying ice type accurately. Sensor Actuator Phys. *175*, 35–42. https://doi.org/10.1016/j.sna.2011.12.016.

20. Dongo, P.D., Machrafi, H., Minetti, C., Amato, A., Queeckers, P., and Iorio, C.S. (2021). A heat-pulse method for detecting ice formation on surfaces. Therm. Sci. Eng. Prog. *22*, 100813. https://doi.org/10.1016/j.tsep.2020.100813.

21. Shi, H., Song, M., Chen, B., Ge, J., Zhang, L., and Zhang, X. (2025). High precision saltwater ice thickness detection method with different salinity under saltwater cover on a horizontal cold plate. Appl. Therm. Eng. *267*, 125794. https://doi.org/10.1016/j.applthermaleng.2025.125794.

22. Gui, K., Ge, J., Ye, L., and Huang, L. (2019). The piezoelectric road status sensor using the frequency scanning method and machine-learning algorithms. Sensor Actuator Phys. *287*, 8–20. https://doi.org/10.1016/j.sna.2018.12.048.

23. He, Q., Li, K., Xu, Z., Wang, J., Wang, X., and Li, A. (2023). Research progress on construction strategy and technical evaluation of aircraft icing accretion protection system. Chin. J. Aeronaut. *36*, 1–23. https://doi.org/10.1016/j.cja.2023.07.003.

24. Aguiar, M., Gaspar, P.D., and da Silva, P.D. (2022). Image recognition method for frost sensing applications. Energy Rep. *8*, 234–240. https://doi.org/10.1016/j.egyr.2022.01.049.

25. Gui, K., Zhou, Y., Bai, H., Ge, J., Song, M., Li, R., and Ye, L. (2025). Flexible ice detection film utilizing arrayed complex impedance sensors. Measurement *245*, 116637. https://doi.org/10.1016/j.measurement.2024.116637.

26. Maio, L., Memmolo, V., Christophel, N., Kohl, S., and Moll, J. (2023). Electromechanical admittance method to monitor ice accretion on a composite plate. Measurement *220*, 113290. https://doi.org/10.1016/j.measurement.2023.113290.

27. Zhao, X., and Rose, J.L. (2016). Ultrasonic guided wave tomography for ice detection. Ultrasonics *67*, 212–219. https://doi.org/10.1016/j.ultras.2015.12.005.

28. Abdalati, W., and Steffen, K. (1995). Passive microwave-derived snow melt regions on the Greenland Ice Sheet. Geophys. Res. Lett. *22*, 787–790. https://doi.org/10.1029/95GL00433.

29. Bulusu, R., and Dhekne, A. (2025). uThaw: Ultra-Wideband Wireless Solid–Liquid State Transition Sensor to Detect Thawing of Food. IEEE Sens. Lett. *9*, 1–4. https://doi.org/10.1109/LSENS.2025.3537922.

30. Liu, X., Small, J., Berdy, D., Katehi, L.P.B., Chappell, W.J., and Peroulis, D. (2011). Impact of Mechanical Vibration on the Performance of RF MEMS Evanescent-Mode Tunable Resonators. IEEE Microw. Wirel. Compon. Lett. *21*, 406–408. https://doi.org/10.1109/LMWC.2011.2160159.

31. Li, Q., Yao, R., Tan, V.B.C., He, F., Zhao, H., and Bai, T. (2025). A review of efficient thermal application for ice detection and anti/de-icing technology. Appl. Therm. Eng. *263*, 125366. https://doi.org/10.1016/j.applthermaleng.2024.125366.

32. Yousuf, A., Khawaja, H., and Virk, M.S. (2024). A review of infrared thermography applications for ice detection and mitigation. Cold Reg. Sci. Technol. *218*, 104058. https://doi.org/10.1016/j.coldregions.2023.104058.

33. Wang, Y., Zhang, Y., Wang, Y., Zhu, D., Zhao, N., and Zhu, C. (2022). Quantitative Measurement Method for Ice Roughness on an Aircraft Surface. Aerospace *9*, 739. https://doi.org/10.3390/aerospace9120739.

34. Zhang, Y., Ge, J., Gui, K., Li, R., and Ye, L. (2025). Mixed-phase measurement during atmospheric icing using ultrasonic pulse-echo (UPE) and signal separation techniques. Measurement *245*, 116679. https://doi.org/10.1016/j.measurement.2025.116679.

35. Ge, J., Li, L., Zhang, Y., Gui, K., and Ye, L. (2025). Ice type identification during dynamic icing process based on ultrasonic pulse echo technique. Sensor Actuator Phys. *393*, 116817. https://doi.org/10.1016/j.sna.2025.116817.

36. Smirnov, A., Anisimkin, V., Ageykin, N., Datsuk, E., and Kuznetsova, I. (2024). Influence of Lamb Wave Anisotropy on Detection of Water-to-Ice Phase Transition. Sensors (Basel) *24*, 7969. https://doi.org/10.3390/s24247969.

37. Bassett, C., Lavery, A.C., Lyons, A.P., Wilkinson, J.P., and Maksym, T. (2020). Direct inference of first-year sea ice thickness using broadband acoustic backscattering. J. Acoust. Soc. Am. *147*, 824–838. https://doi.org/10.1121/10.0000619.

38. Ghobrial, T.R., Loewen, M.R., and Hicks, F.E. (2013). Continuous monitoring of river surface ice during freeze-up using upward looking sonar. Cold Reg. Sci. Technol. *86*, 69–85. https://doi.org/10.1016/j.coldregions.2012.10.009.

39. Hansman, R.J., and Kirby, M.S. (1986). Measurement of ice growth during simulated and natural icing conditions using ultrasonic pulse-echo techniques. J. Aircr. *23*, 492–498. https://doi.org/10.2514/3.45334.

40. Hansman, R.J., and Kirby, M.S. (1985). Measurement of ice accretion using ultrasonic pulse-echo techniques. J. Aircr. *22*, 530–535. https://doi.org/10.2514/3.45160.

41. Zhou, N., Song, P., Zhang, Y., and Zhu, C. (2024). Design of high-precision multi-channel ice detection system. J. Phys, Conf. Ser. *2897*, 012019. https://doi.org/10.1088/1742-6596/2897/1/012019.

42. Wang, Y., Wang, Y., Li, W., Wu, D., Zhao, N., and Zhu, C. (2022). Study on freezing characteristics of the surface water film over glaze ice by using an ultrasonic pulse-echo technique. Ultrasonics *126*, 106804. https://doi.org/10.1016/j.ultras.2022.106804.

43. Liu, Y., Chen, W.-L., Bond, L.J., and Hu, H. (2014). Development of an ultrasonic pulse-echo (UPE) technique for aircraft icing studies. AIP Conf. Proc. *1581*, 1757–1764. https://doi.org/10.1063/1.4865036.

44. GUI, K., ZHANG, Y., GE, J., LI, R., and YE, L. (2023). Ice Porosity Measurement Utilizing Dynamic Wavelet Fingerprint Technology

(Transactions of Nanjing University of Aeronautics & Astronautics), pp. 118–128. https://doi.org/10.16356/j.1005-1120.2023.S1.011.

45. Zeng, X., Ong, H., Haworth, L., Lu, Y., Yang, D., Rahmati, M., Wu, Q., Torun, H., Martin, J., Hou, X., et al. (2023). Fundamentals of Monitoring Condensation and Frost/Ice Formation in Cold Environments Using Thin-Film Surface-Acoustic-Wave Technology. ACS Appl. Mater. Interfaces *15*, 35648–35663. https://doi.org/10.1021/acsami.3c04854.
46. Maio, L., Moll, J., Memmolo, V., and Simon, J. (2022). Ultrasonic inspection for ice accretion assessment: effects on direct wave propagation in composite media. Mech. Syst. Signal Process. *173*, 109025. https://doi.org/10.1016/j.ymssp.2022.109025.
47. Zhao, Z., Yin, Y., Cui, B., and Wang, W. (2025). Modeling and simulation of the influence mechanism of ice accretion on SAW propagation. AIP Adv. *15*, 095223. https://doi.org/10.1063/5.0264981.
48. del Moral, J., Haworth, L., Montes, L., Sánchez-Valencia, J.R., Barranco, A., Rico, V.J., Czermak, T., Carreño, F., García-Gallego, P., Mora, J., et al. (2026). Acoustic Wave-Powered Durable Icephobic Duplex Coating Design with Superior Deicing Performance. ACS Appl. Mater. Interfaces *18*, 9018–9031. https://doi.org/10.1021/acsami.5c19758.
49. Gao, H., and Rose, J.L. (2009). Ice detection and classification on an aircraft wing with ultrasonic shear horizontal guided waves. IEEE Trans. Ultrason. Ferroelectr. Freq. Control *56*, 334–344. https://doi.org/10.1109/TUFFC.2009.1042.
50. Mendig, C., Riemenschneider, J., Monner, H.P., Vier, L.J., Endres, M., and Sommerwerk, H. (2018). Ice detection by ultrasonic guided waves. CEAS Aeronaut. J. *9*, 405–415. https://doi.org/10.1007/s13272-018-0289-0.
51. Jiménez, A.A., García Márquez, F.P., Moraleda, V.B., and Gómez Muñoz, C.Q. (2019). Linear and nonlinear features and machine learning for wind turbine blade ice detection and diagnosis. Renew. Energy *132*, 1034–1048. https://doi.org/10.1016/j.renene.2018.08.050.
52. Zhou, C., Su, Z., and Cheng, L. (2011). Probability-based diagnostic imaging using hybrid features extracted from ultrasonic Lamb wave signals. Smart Mater. Struct. *20*, 125005. https://doi.org/10.1088/0964-1726/20/12/125005.
53. Marko, J.R., and Jasek, M. (2010). Sonar detection and measurements of ice in a freezing river I: Methods and data characteristics. Cold Reg. Sci. Technol. *63*, 121–134. https://doi.org/10.1016/j.coldregions.2010.05.005.
54. McLaren, A.S. (1989). The under-ice thickness distribution of the Arctic Basin as recorded in 1958 and 1970. J. Geophys. Res. *94*, 4971–4983. https://doi.org/10.1029/JC094iC04p04971.
55. Wadhams, P., and Horne, R.J. (1980). An analysis of ice profiles obtained by submarine sonar in the beaufort sea. J. Glaciol. *25*, 401–424. https://doi.org/10.3189/S0022143000015264.
56. Fissel, D.B., Marko, J.R., Ross, E., Lee, V., Chave, R.A.J., and Egan, J. (2007). Improvements in upward looking sonar-based sea-ice measurements: A case study for 2007 ice features in Northumberland strait, Canada. Oceans *1–6*, 1–6. https://doi.org/10.1109/OCEANS.2007.4449194.
57. Belliveau, D.J., Hayden, H., and Prinsenberg, S. (2001). Ice drift and draft measurements from moorings at the confederation bridge. In Proceedings of the International Conference on Port and Ocean Engineering Under Arctic Conditions.
58. Hudson, R. (1990). Annual measurement of sea-ice thickness using an upward-looking sonar. Nature *344*, 135–137. https://doi.org/10.1038/344135a0.
59. Behrendt, A., Dierking, W., Fahrbach, E., and Witte, H. (2013). Sea ice draft in the Weddell Sea, measured by upward looking sonars. Earth Syst. Sci. Data *5*, 209–226. https://doi.org/10.5194/essd-5-209-2013.
60. Khvorostovsky, K., Hendricks, S., and Rinne, E. (2020). Surface Properties Linked to Retrieval Uncertainty of Satellite Sea-Ice Thickness with Upward-Looking Sonar Measurements. Remote Sens. *12*, 3094. https://doi.org/10.3390/rs12183094.
61. Lucieer, V., Nau, A., Forrest, A., and Hawes, I. (2016). Fine-Scale Sea Ice Structure Characterized Using Underwater Acoustic Methods. Remote Sens. *8*, 821. https://doi.org/10.3390/rs8100821.
62. Ghobrial, T.R., Loewen, M.R., and Hicks, F.E. (2013). Characterizing suspended frazil ice in rivers using upward looking sonars. Cold Reg. Sci. Technol. *86*, 113–126. https://doi.org/10.1016/j.coldregions.2012.10.002.
63. Wang, Y., Wang, Y., Chen, S., Zhu, C., Wu, D., Zhu, C., and Lu, X. (2025). Focused ultrasonic transducer for aircraft icing detection. Ultrasonics *147*, 107509. https://doi.org/10.1016/j.ultras.2024.107509.
64. Rizk, P., Younes, R., Ilinca, A., and Khoder, J. (2022). Wind turbine ice detection using hyperspectral imaging. Remote Sens. Appl.: Soc. Environ. *26*, 100711. https://doi.org/10.1016/j.rsase.2022.100711.
65. Ikiades, A.A., Armstrong, D.J., and Howard, G. (2007). Optical diffusion and polarization characteristics of ice accreting in dynamic conditions using a backscattering fibre optic technique. Sensor Actuator Phys. *140*, 43–50. https://doi.org/10.1016/j.sna.2007.06.009.
66. Hu, Q., Xu, X., Leng, D., Shu, L., Jiang, X., Virk, M., and Yin, P. (2021). A method for measuring ice thickness of wind turbine blades based on edge detection. Cold Reg. Sci. Technol. *192*, 103398. https://doi.org/10.1016/j.coldregions.2021.103398.
67. Yamada, M., Ueda, K., Horiba, I., and Sugie, N. (2001). Discrimination of the road condition toward understanding of vehicle driving environments. IEEE trans. Intell. Transp. Syst. *2*, 26–31. https://doi.org/10.1109/6979.911083.
68. Šabanovič, E., Žuraulis, V., Prentkovskis, O., and Skrickij, V. (2020). Identification of Road-Surface Type Using Deep Neural Networks for Friction Coefficient Estimation. Sensors (Basel) *20*, 612. https://doi.org/10.3390/s20030612.
69. Abdel-Moati, H., Morris, J., Zeng, Y., Corie, M.W., and Yanni, V.G. (2018). Near field ice detection using infrared based optical imaging technology. Opt. Laser Technol. *99*, 402–410. https://doi.org/10.1016/j.optlastec.2017.09.029.
70. Li, W., Zhang, J., Ye, L., and Zhang, H. (2009). A Fiber-Optic Solution to Aircraft Icing Detection and Measurement Problem. 2009 Int. Conf. Inf. Tech. Comput. Sci. *1*, 357–360. https://doi.org/10.1109/ITCS.2009.77.
71. Zhang, C., Xiao, C., Li, S., Guo, X., Wang, Q., He, Y., Lv, H., Yan, H., and Liu, D. (2023). A Novel Fiber-Optic Ice Sensor to Identify Ice Types Based on Total Reflection. Sensors (Basel) *23*, 3996. https://doi.org/10.3390/s23083996.
72. Xie, J., Zeng, X., Ni, S., Chu, R., Liang, C., Chi, B., Bao, F., and Song, Z. (2025). Using distributed fiber optic sensing data to invert for the properties of the ice layer. Chinese J. Geophy.-Chinese Edition *68*, 153–163. https://doi.org/10.6038/cjg2024R0583.
73. Zou, J., Ye, L., Ge, J., and Zhao, C. (2013). Novel fiber optic sensor for ice type detection. Measurement *46*, 881–886. https://doi.org/10.1016/j.measurement.2012.09.020.
74. Ikiades, A. (2022). Fiber Optic Ice Sensor for Measuring Ice Thickness, Type and the Freezing Fraction on Aircraft Wings. Aerospace *10*, 31. https://doi.org/10.3390/aerospace10010031.
75. Ge, J., Liu, J., Gui, K., and Ye, L. (2022). Atmospheric icing measurement and online ice type recognition for aircraft utilizing optical fiber sensor and machine learning algorithms. Measurement *205*, 112215. https://doi.org/10.1016/j.measurement.2022.112215.
76. Kreutz, M., Alla, A.A., Eisenstadt, A., Freitag, M., and Thoben, K.-D. (2020). Ice Detection on Rotor Blades of Wind Turbines using RGB Images and Convolutional Neural Networks. Proced. CIRP *93*, 1292–1297. https://doi.org/10.1016/j.procir.2020.04.107.
77. Moroto, Y., Maeda, K., Ogawa, T., and Haseyama, M. (2024). Snow- or ice-covered road detection in winter road surface conditions using

deep neural networks. Comput. Aided Civ. Infrastruct. Eng. *39*, 2935–2950. https://doi.org/10.1111/mice.13233.

78. Jokela, M., Kutila, M., and Le, L. (2009). Road condition monitoring system based on a stereo camera. In 2009 IEEE 5th International Conference on Intelligent Computer Communication and Processing, pp. 423–428. https://doi.org/10.1109/ICCP.2009.5284724.
79. Ansari, S., Rennie, C.D., Seidou, O., Malenchak, J., and Zare, S.G. (2017). Automated monitoring of river ice processes using shore-based imagery. Cold Reg. Sci. Technol. *142*, 1–16. https://doi.org/10.1016/j.coldregions.2017.06.011.
80. Wright, N.C., Polashenski, C.M., McMichael, S.T., and Beyer, R.A. (2020). Observations of sea ice melt from Operation IceBridge imagery. Cryosphere *14*, 3523–3536. https://doi.org/10.5194/tc-14-3523-2020.
81. Zheng, X., Shi, R., You, S., Han, Y., and Shi, K. (2019). Experimental study of defrosting control method based on image processing technology for air source heat pumps. Sustain. Cities Soc. *51*, 101667. https://doi.org/10.1016/j.scs.2019.101667.
82. Li, Z., Wang, W., Sun, Y., Wang, S., Deng, S., and Lin, Y. (2021). Applying image recognition to frost built-up detection in air source heat pumps. Energy *233*, 121004. https://doi.org/10.1016/j.energy.2021.121004.
83. Hu, M., He, J., and Alsabaan, M. (2023). Image Identification Method of Ice Thickness on Transmission Line Based on Visual Sensing. Mob. Netw. Appl. *28*, 1783–1792. https://doi.org/10.1007/s11036-023-02244-1.
84. Dai, D., Hu, Y., Qian, H., Qi, G., and Wang, Y. (2024). A Novel Detection Algorithm for the Icing Status of Transmission Lines. Symmetry *16*, 1264. https://doi.org/10.3390/sym16101264.
85. Ishii, Y., Fuchida, M., Ozeki, K., and Nakamura, A. (2025). Investigation on the Use of Polarized Images for Frozen Road Surface Recognition. In 2025 IEEE/SICE International Symposium on System Integration (SII), pp. 1581–1586. https://doi.org/10.1109/SII59315.2025.10870979.
86. Nguyen, C.V., Milford, M., and Mahony, R. (2017). 3D tracking of water hazards with polarized stereo cameras. In 2017 IEEE International Conference on Robotics and Automation (ICRA), pp. 5251–5257. https://doi.org/10.1109/ICRA.2017.7989616.
87. Casselgren, J., Rosendahl, S., Sjödahl, M., and Jonsson, P. (2016). Road condition analysis using NIR illumination and compensating for surrounding light. Opt. Lasers Eng. *77*, 175–182. https://doi.org/10.1016/j.optlaseng.2015.08.002.
88. Colace, L., Santoni, F., and Assanto, G. (2013). A near-infrared optoelectronic approach to detection of road conditions. Opt. Lasers Eng. *51*, 633–636. https://doi.org/10.1016/j.optlaseng.2013.01.003.
89. Buckley, E.M., Farrell, S.L., Duncan, K., Connor, L.N., Kuhn, J.M., and Dominguez, R.T. (2020). Classification of Sea Ice Summer Melt Features in High-Resolution IceBridge Imagery. JGR. Oceans *125*, e2019JC015738. https://doi.org/10.1029/2019JC015738.
90. Riehm, M., Gustavsson, T., Bogren, J., and Jansson, P.-E. (2012). Ice formation detection on road surfaces using infrared thermometry. Cold Reg. Sci. Technol. *83–84*, 71–76. https://doi.org/10.1016/j.coldregions.2012.06.004.
91. Rieman, L., Guk, E., Kim, T., Son, C., and Kim, J.-S. (2020). Development of a Novel Multi-Channel Thermocouple Array Sensor for In-Situ Monitoring of Ice Accretion. Sensors (Basel) *20*, 2165. https://doi.org/10.3390/s20082165.
92. Gonzalez del Val, M., and Frövel, M. (2024). Flight tests results of a Fiber Bragg Gratings based ice sensor. Cold Reg. Sci. Technol. *224*, 104248. https://doi.org/10.1016/j.coldregions.2024.104248.
93. Guk, E., Son, C., Rieman, L., and Kim, T. (2021). Experimental study on ice intensity and type detection for wind turbine blades with multi-channel thermocouple array sensor. Cold Reg. Sci. Technol. *189*, 103297. https://doi.org/10.1016/j.coldregions.2021.103297.
94. King, W.D., Parkin, D.A., and Handsworth, R.J. (1978). A Hot-Wire Liquid Water Device Having Fully Calculable Response Characteristics. J. Appl. Meteor. *17*, 1809–1813. https://doi.org/10.1175/1520-0450(1978)017<1809:ahwlwd>2.0.co;2.
95. Korolev, A.V., Strapp, J.W., Isaac, G.A., and Nevzorov, A.N. (1998). The Nevzorov Airborne Hot-Wire LWC–TWC Probe: Principle of Operation and Performance Characteristics. J. Atmos. Ocean. Technol. *15*, 1495–1510. https://doi.org/10.1175/1520-0426(1998)015<1495:tnahwl>2.0.co;2.
96. Lucke, J., Jurkat-Witschas, T., Heller, R., Hahn, V., Hamman, M., Breitfuss, W., Bora, V.R., Moser, M., and Voigt, C. (2022). Icing wind tunnel measurements of supercooled large droplets using the 12 mm total water content cone of the Nevzorov probe. Atmos. Meas. Tech. *15*, 7375–7394. https://doi.org/10.5194/amt-15-7375-2022.
97. Korolev, A., Strapp, J.W., Isaac, G.A., and Emery, E. (2013). Improved Airborne Hot-Wire Measurements of Ice Water Content in Clouds. J. Atmos. Ocean. Technol. *30*, 2121–2131. https://doi.org/10.1175/JTECH-D-13-00007.1.
98. Ye, Y., Wang, X., Sun, S., Liu, Q., Li, X., Cheng, X., and Chen, Z. (2024). A new sea ice concentration retrieval algorithm from thermal infrared imagery. Int. J. Digit. Earth *17*, 2353116. https://doi.org/10.1080/17538947.2024.2353116.
99. Tian, Z., Ren, T., Kojima, Y., Lu, Y., Horton, R., and Heitman, J.L. (2017). An improved thermo-time domain reflectometry method for determination of ice contents in partially frozen soils. J. Hydrol. (Amst). *555*, 786–796. https://doi.org/10.1016/j.jhydrol.2017.10.055.
100. Zhang, T.T., Wang, S., and Wang, F. (2024). Adopting a hot film to measure thickness of an ice layer under sweeping wind. Int. Commun. Heat Mass Transf. *154*, 107453. https://doi.org/10.1016/j.icheatmasstransfer.2024.107453.
101. Liao, Z., Cheng, Y., Jiang, Y., Li, M., Cheng, B., and Sandven, S. (2023). Ice bottom evolution derived from thermistor string-based ice mass balance buoy observations. Int. J. Digit. Earth *16*, 3085–3104. https://doi.org/10.1080/17538947.2023.2242326.
102. Willmes, S., and Heinemann, G. (2015). Sea-Ice Wintertime Lead Frequencies and Regional Characteristics in the Arctic, 2003–2015. Remote Sens. *8*, 4. https://doi.org/10.3390/rs8010004.
103. Ludwig, V., Spreen, G., Haas, C., Istomina, L., Kauker, F., and Murashkin, D. (2019). The 2018 North Greenland polynya observed by a newly introduced merged optical and passive microwave sea-ice concentration dataset. Cryosphere *13*, 2051–2073. https://doi.org/10.5194/tc-13-2051-2019.
104. Paul, S., and Huntemann, M. (2021). Improved machine-learning-based open-water–sea-ice–cloud discrimination over wintertime Antarctic sea ice using MODIS thermal-infrared imagery. Cryosphere *15*, 1551–1565. https://doi.org/10.5194/tc-15-1551-2021.
105. Drüe, C., and Heinemann, G. (2004). High-resolution maps of the sea-ice concentration from MODIS satellite data. Geophys. Res. Lett. *31*, L20403. https://doi.org/10.1029/2004GL020808.
106. Shi, W., Yuan, S., Liu, C., Ma, Y., Xu, N., and Lv, X. (2022). Inversion of Sea Ice Concentration in the Liaodong Bay from MODIS Data. Remote Sens. *14*, 4439. https://doi.org/10.3390/rs14184439.
107. Zhang, H., Yao, X., Wei, Q., Duan, H., and Zhang, Y. (2022). Comparison of Lake Ice Extraction Methods Based on MODIS Images. Remote Sens. *14*, 4740. https://doi.org/10.3390/rs14194740.
108. Che, J., Ding, M., Zhang, Q., Wang, Y., Sun, W., Wang, Y., Wang, L., and Huai, B. (2022). Reconstruction of Near-Surface Air Temperature over the Greenland Ice Sheet Based on MODIS Data and Machine Learning Approaches. Remote Sens. *14*, 5775. https://doi.org/10.3390/rs14225775.
109. Shimada, R., Takeuchi, N., and Aoki, T. (2016). Inter-Annual and Geographical Variations in the Extent of Bare Ice and Dark Ice on the Greenland Ice Sheet Derived from MODIS Satellite Images. Front. Earth Sci. *4*, 43. https://doi.org/10.3389/feart.2016.00043.
110. Preußer, A., Heinemann, G., Willmes, S., and Paul, S. (2015). Multi-Decadal Variability of Polynya Characteristics and Ice Production in the

North Water Polynya by Means of Passive Microwave and Thermal Infrared Satellite Imagery. Remote Sens. *7*, 15844–15867. https://doi.org/10.3390/rs71215807.

111. Nalli, N.R., Dang, C., Jung, J.A., Knuteson, R.O., Borbas, E.E., Johnson, B.T., Pryor, K., and Zhou, L. (2023). Physically Based Thermal Infrared Snow/Ice Surface Emissivity for Fast Radiative Transfer Models. Remote Sens. *15*, 5509. https://doi.org/10.3390/rs15235509.
112. Gómez Muñoz, C.Q., García Márquez, F.P., and Sánchez Tomás, J.M. (2016). Ice detection using thermal infrared radiometry on wind turbine blades. Measurement *93*, 157–163. https://doi.org/10.1016/j.measurement.2016.06.064.
113. Madi, E., Pope, K., and Huang, W. (2022). An integrated ice tracking and mitigation system on the stagnation line of a cylindrical surface based on thermal imaging and electro-thermal elements. Measurement *199*, 111539. https://doi.org/10.1016/j.measurement.2022.111539.
114. Wang, K., Wang, G., Chen, H., Wan, S., and Lv, C. (2019). Quantitative identification of three-dimensional subsurface defect based on the fuzzy inference of thermal process. Int. J. Heat Mass Transf. *133*, 903–911. https://doi.org/10.1016/j.ijheatmasstransfer.2018.12.149.
115. Li, Q., Hao, L., Pan, W., Liu, S., and Bai, T. (2022). Three-dimensional ice shape detection based on flash pulse infrared thermal wave testing. Case Stud. Therm. Eng. *36*, 102196. https://doi.org/10.1016/j.csite.2022.102196.
116. Zhang, C., Nateghinia, E., Miranda-Moreno, L.F., and Sun, L. (2022). Winter road surface condition classification using convolutional neural network (CNN): visible light and thermal image fusion. Can. J. Civ. Eng. *49*, 569–578. https://doi.org/10.1139/cjce-2020-0613.
117. Troiano, A., Pasero, E., and Mesin, L. (2011). New System for Detecting Road Ice Formation. IEEE Trans. Instrum. Meas. *60*, 1091–1101. https://doi.org/10.1109/TIM.2010.2064910.
118. Dean, R.N. (2021). A PCB Sensor for Detecting Icing Events. IEEE Sens. Lett. *5*, 1–4. https://doi.org/10.1109/LSENS.2020.3046947.
119. Adams, D.J. (1981). Theory of the dielectric constant of ice. Nature *293*, 447–449. https://doi.org/10.1038/293447a0.
120. Shi, H., Song, M., Kim, D.R., Lu, P., Zhang, X., and Zhang, L. (2025). Experimental study on the location detection method of deionized water freezing front based on microwave resonance theory. Measurement *242*, 115859. https://doi.org/10.1016/j.measurement.2024.115859.
121. Abdelaal, A., Sarayloo, M., Nims, D.K., Mohammadian, B., Heil, J., and Sojoudi, H. (2022). A flexible surface-mountable sensor for ice detection and non-destructive measurement of liquid water content in snow. Cold Reg. Sci. Technol. *195*, 103469. https://doi.org/10.1016/j.coldregions.2021.103469.
122. Abie, S.M., Münch, D., and Bergli, J. (2020). Monitoring Electric Impedance During Freezing and Thawing of Saline and De-ionized Water. J. Electr. Bioimpedance *11*, 106–111. https://doi.org/10.2478/joeb-2020-0016.
123. Tabatabai, H., and Aljuboori, M. (2017). A Novel Concrete-Based Sensor for Detection of Ice and Water on Roads and Bridges. Sensors (Basel) *17*, 2912. https://doi.org/10.3390/s17122912.
124. Zhi, X., Cho, H.C., Wang, B., Ahn, C.H., Moon, H.S., and Go, J.S. (2015). Development of a Capacitive Ice Sensor to Measure Ice Growth in Real Time. Sensors (Basel) *15*, 6688–6698. https://doi.org/10.3390/s150306688.
125. Wagih, M., and Shi, J. (2022). Toward the Optimal Antenna-Based Wireless Sensing Strategy: An Ice Sensing Case Study. IEEE Open J. Antennas Propag. *3*, 687–699. https://doi.org/10.1109/OJAP.2022.3182770.
126. Gui, K., Liu, J., Ge, J., Li, H., and Ye, L. (2022). Atmospheric icing process measurement utilizing impedance spectroscopy and thin film structure. Measurement *202*, 111851. https://doi.org/10.1016/j.measurement.2022.111851.
127. Ur Rahman, H., Naeem Malik, A., and Lazoglu, I. (2024). Ice growth detection and the de-icing using dual functional capacitive sensor. Measurement *237*, 115208. https://doi.org/10.1016/j.measurement.2024.115208.
128. Elzaidi, A., Masek, V., and Muzychka, Y. (2019). Phase Discrimination in Marine Icing Using a Coplanar Capacitive Array. IEEE Sens. J. *19*, 11301–11308. https://doi.org/10.1109/JSEN.2019.2935616.
129. Gui, K., Bai, H., Liu, Z., Ge, J., and Ye, L. (2023). Impedance Ice Sensor Capable of Self-Componsating Temperature Drift. In 2023 IEEE 16th International Conference on Electronic Measurement & Instruments (ICEMI), pp. 118–122. https://doi.org/10.1109/ICEMI59194.2023.10270421.
130. Jiang, J., Xu, G., Wang, H., Yang, Z., Sun, B., Guan, C., Feng, J., Ma, Y., and Chen, X. (2024). High-accuracy road surface condition detection through multi-sensor information fusion based on WOA-BP neural network. Sensor Actuator Phys. *378*, 115829. https://doi.org/10.1016/j.sna.2024.115829.
131. Zhang, X., Zhou, W., and Li, H. (2019). Electromechanical impedance-based ice detection of stay cables with temperature compensation. Struct. Control Health Monit. *26*, 115859. https://doi.org/10.1002/stc.2384.
132. Zheng, D., Li, Z., Du, Z., Ma, Y., Zhang, L., Du, C., Li, Z., Cui, L., Zhang, L., Xuan, X., and Deng, X. (2022). Design of Capacitance and Impedance Dual-Parameters Planar Electrode Sensor for Thin Ice Detection of Aircraft Wings. IEEE Sens. J. *22*, 11006–11015. https://doi.org/10.1109/JSEN.2022.3169477.
133. Lu, B., Zhao, H., Ma, J., Wang, J., Li, Q., Xun, W., and Wu, D. (2025). Electrothermal-coupled flexible microwave resonant icing sensor Array. Microelectron. Eng. *300*, 112360. https://doi.org/10.1016/j.mee.2025.112360.
134. Altrabolsi, M., Saleh, M., Elhajj, I.H., and Asmar, D. (2025). A planar capacitive sensor for detecting and measuring thickness and depth of oil under ice. Meas. Sci. Technol. *36*, 015809. https://doi.org/10.1088/1361-6501/ad99ee.
135. Inanlu, M.J., Gurumukhi, Y., Kabirzadeh, P., Anand, R., Khodakarami, S., Viswanathan, V., Stillwell, A., and Miljkovic, N. (2024). Capacitive sensing of frost growth dynamics on aluminum surfaces with different wettabilities. Int. J. Heat Mass Transf. *225*, 125377. https://doi.org/10.1016/j.ijheatmasstransfer.2024.125377.
136. Flatscher, M., Neumayer, M., and Bretterklieber, T. (2017). Field sensor analysis for electrical impedance spectroscopy based ice detection. 2017. IEEE SENSORS, 1–3. https://doi.org/10.1109/ICSENS.2017.8234035.
137. Xie, J., Wen, J., Chen, J., and Yuan, W. (2022). Microwave Icing Sensor Based on Interdigital-Complementary Split-Ring Resonator. IEEE Sens. J. *22*, 12829–12837. https://doi.org/10.1109/JSEN.2022.3176932.
138. Tariq, R.U., Ye, M., Zhao, X.-L., Zhang, S.-C., Cao, Z., and He, Y.-N. (2021). Microwave Sensor for Detection of Ice Accretion on Base Station Antenna Radome. IEEE Sens. J. *21*, 18733–18741. https://doi.org/10.1109/JSEN.2021.3089320.
139. Kozak, R., Khorsand, K., Zarifi, T., Golovin, K., and Zarifi, M.H. (2021). Patch antenna sensor for wireless ice and frost detection. Sci. Rep. *11*, 13707. https://doi.org/10.1038/s41598-021-93082-2.
140. Shi, H., Song, M., Ge, J., Zhang, L., and Zhang, X. (2025). A high-precision saltwater ice thickness and salinity detection method based on capacitive coupled planar microwave resonator. Cold Reg. Sci. Technol. *231*, 104417. https://doi.org/10.1016/j.coldregions.2024.104417.
141. Wiltshire, B., Mirshahidi, K., Golovin, K., and Zarifi, M.H. (2019). Robust and sensitive frost and ice detection via planar microwave resonator sensor. Sensor. Actuator. B Chem. *301*, 126881. https://doi.org/10.1016/j.snb.2019.126881.
142. Shi, H., Song, M., Narita, F., Hosseini, S.H., Zhang, L., and Chao, C.Y.H. (2025). Experimental study on high-precision detection technology for the freezing front height in brine on a horizontal cold plate surface in

cold regions. Renew. Energy *246*, 122928. https://doi.org/10.1016/j.renene.2025.122928.

143. Niksan, O., Colegrave, K., and Zarifi, M.H. (2023). Battery-Free, Artificial Neural Network-Assisted Microwave Resonator Array for Ice Detection. IEEE Trans. Microw. Theory Tech. *71*, 698–709. https://doi.org/10.1109/TMTT.2022.3222194.

144. Jones, K., Ingham, M., Pringle, D., and Eicken, H. (2011). Cross-borehole resistivity tomography of Arctic and Antarctic sea ice. Ann. Glaciol. *52*, 161–168. https://doi.org/10.3189/172756411795931723.

145. Barsukov, P.O., and Fainberg, E.B. (2020). Mapping bedrock topography and moraine deposits by transient electromagnetic sounding: Oslo graben, Norway. Near Surf. Geophys. *18*, 123–133. https://doi.org/10.1002/nsg.12070.

146. Mudler, J., Hördt, A., Przyklenk, A., Fiandaca, G., Maurya, P.K., and Hauck, C. (2019). Two-dimensional inversion of wideband spectral data from the capacitively coupled resistivity method – first applications in periglacial environments. Cryosphere *13*, 2439–2456. https://doi.org/10.5194/tc-13-2439-2019.

147. Phillips, M., Buchli, C., Weber, S., Boaga, J., Pavoni, M., and Bast, A. (2023). Brief communication: Combining borehole temperature, borehole piezometer and cross-borehole electrical resistivity tomography measurements to investigate seasonal changes in ice-rich mountain permafrost. Cryosphere *17*, 753–760. https://doi.org/10.5194/tc-17-753-2023.

148. Kristensen, L., Juliussen, H., Christiansen, H.H., and Humlum, O. (2009). Structure and composition of a tidewater glacier push moraine, Svalbard, revealed by DC resistivity profiling. Boreas *38*, 176–186. https://doi.org/10.1111/j.1502-3885.2008.00045.x.

149. Shi, Q., Wang, J.B., Chen, D.Y., and Shang, Y.L. (2012). A Flush-Mounted Resonant Ice Detection Sensor with High Sensitivity. Key Eng. Mater. *503*, 81–86. https://doi.org/10.4028/www.scientific.net/KEM.503.81.

150. Mäder, T., Nestler, M., Kranz, B., and Drossel, W.-G. (2018). Studies on Sheet-Metal Compounds with Piezoceramic Modules for Icing Detection and De-Icing. Adv. Eng. Mater. *20*, 1800589. https://doi.org/10.1002/adem.201800589.

151. Han, N., Siddique, M.A., Zhang, Z., Tian, L., Hu, H., and Hu, H. (2023). A flight-testing campaign to examine inflight icing characteristics and its effects on the flight performance of an Unmanned-Aerial-Vehicle. Cold Reg. Sci. Technol. *207*, 103775. https://doi.org/10.1016/j.coldregions.2023.103775.

152. Palanque, V., Planès, T., Pommier-budinger, V., Budinger, M., and Delbecq, S. (2024). Piezoelectric resonant ice protection systems Part 2/2: Evaluation of benefits at aircraft level. Chin. J. Aeronaut. *37*, 92. https://doi.org/10.1016/j.cja.2024.03.021.

153. Zhang, L., Du, X., Xu, C., Cheng, P., Zhao, M., Du, C., Cui, L., and Deng, X. (2025). Static ice pressure detection system of FBG loop ring-down cavity based on FPGA. Opt. Fiber Technol. *95*, 104397. https://doi.org/10.1016/j.yofte.2025.104397.

154. Zhang, L., Hu, B., Cheng, P., Cui, L., Du, C., Du, X., Zhao, M., and Xu, C. (2024). Design of fiber Bragg grating sensor for static ice pressure detection. Opt. Fiber Technol. *86*, 103845. https://doi.org/10.1016/j.yofte.2024.103845.

155. Swytink-Binnema, N., Godreau, C., and Arbez, C. (2019). Detecting instrumental icing using automated double anemometry. Wind Energy *22*, 80–88. https://doi.org/10.1002/we.2271.

156. Tammelin, B., Böhringer, A., Cavaliere, M., Holttinen, H., Morgan, C., Seifert, H., Säntti, K., and Vølund, P. (2000). Wind Energy Production in Cold Climate (WECO) (Finnish Meteorological Institute).

157. Zhao, Y., Gui, K., Du, W., Ge, J., Chen, M., and Ye, L. (2020). Principle and Experimental Study of Icing Condition Sensor for EMU Train. Tie Dao Xue Bao *42*, 60–66. https://doi.org/10.3969/j.issn.1001-8360.2020.10.009.

158. Wang, Y., Wang, Y., Lu, Q., Zhu, C., Wu, D., Zhu, C., and Wu, Y. (2025). A Flexible Ultra-Thin Ultrasonic Transducer for Ice Detection on Curved Surfaces. Aerospace *12*, 997. https://doi.org/10.3390/aerospace12110997.

159. Farina, D., Mazio, M., Machrafi, H., Queeckers, P., and Iorio, C.S. (2024). Environmental Chamber Characterization of an Ice Detection Sensor for Aviation Using Graphene and PEDOT:PSS. Micromachines *15*, 504. https://doi.org/10.3390/mi15040504.

160. Sibilia, S., Tari, L., Bertocchi, F., Chiodini, S., and Maffucci, A. (2023). A Capacitive Ice-Sensor Based on Graphene Nano-Platelets Strips. Sensors (Basel) *23*, 9877. https://doi.org/10.3390/s23249877.

161. Dongo, P.D., Hakansson, A., Stoeckel, M.-A., Pavlopoulou, E., Wang, S., Farina, D., Queeckers, P., Fabiano, S., Iorio, C.S., and Crispin, R. (2023). Detection of ice formation with the polymeric mixed ionic-electronic conductor PEDOT: PSS for aeronautics. Adv. Electron. Mater. *9*, 2300060. https://doi.org/10.1002/aelm.202300060.

162. Lu, B., Yuk, H., Lin, S., Jian, N., Qu, K., Xu, J., and Zhao, X. (2019). Pure PEDOT:PSS hydrogels. Nat. Commun. *10*, 1043. https://doi.org/10.1038/s41467-019-09003-5.

163. Hou, W., Chen, X., Wang, D., Cao, Y., Du, H., Li, G., Gan, Z., Yan, Y., Gao, C., Hu, F., et al. (2025). Chromatic forecasting hydrogels for anti-icing applications. Nat. Commun. *16*, 4881. https://doi.org/10.1038/s41467-025-58806-2.

164. Tang, X., Luo, K., Dong, S., Zhang, Z., and Sun, B. (2022). Quantifying Basal Roughness and Internal Layer Continuity Index of Ice Sheets by an Integrated Means with Radar Data and Deep Learning. Remote Sens. *14*, 4507. https://doi.org/10.3390/rs14184507.

165. Hong, S.B., Yun, H.S., Yum, S.G., Ryu, S.Y., Jeong, I.S., and Kim, J. (2022). Development of black ice prediction model using GIS-based multi-sensor model validation. Nat. Hazards Earth Syst. Sci. *22*, 3435–3459. https://doi.org/10.5194/nhess-22-3435-2022.

166. Gui, K., Bai, H., Liu, Z., Ge, J., and Ye, L. (2024). Mixed phase measurement during icing process utilizing multi-wavelength interdigital sensor. Appl. Therm. Eng. *242*, 122491. https://doi.org/10.1016/j.applthermaleng.2024.122491.

167. Huang, L., Song, M., Shen, J., Kim, D.R., Zhang, L., and Pekař, L. (2024). Experimental study on the effect of inverted aperture plate temperature on frosting characteristics under rising flow considering edge effect. Int. J. Heat Mass Transf. *224*, 125343. https://doi.org/10.1016/j.ijheatmasstransfer.2024.125343.

168. Huang, L., Song, M., Hosseini, S.H., Gao, F., Zhen, Z., and Chen, N. (2025). Experimental investigation on the effect of air temperature on the anti-frosting effect of wire mesh based on space radiation. Appl. Therm. Eng. *271*, 126316. https://doi.org/10.1016/j.applthermaleng.2025.126316.

169. Bouguettaya, A., Zarzour, H., Kechida, A., and Taberkit, A.M. (2022). Deep learning techniques to classify agricultural crops through UAV imagery: a review. Neural Comput. Appl. *34*, 9511–9536. https://doi.org/10.1007/s00521-022-07104-9.

170. He, L., Huang, Z., Hu, Z., Xu, Z., Gui, K., Ge, J., and Li, Y. (2026). Measuring ice thickness on blades of wind turbines using an electrode array. Measurement *257*, 118977. https://doi.org/10.1016/j.measurement.2025.118977.

171. Golam, M., Md Tayeb, A., Ayesha Khatun, M., Facklasur Rahaman, M., Aouto, A., Paul Angelo, O., Kim, D.-S., Lee, J.-M., and Kim, J.-H. (2025). BlackIceNet: Explainable AI-Enhanced Multimodal for Black Ice Detection to Prevent Accidents in Intelligent Vehicles. IEEE Internet Things J. *12*, 15558–15571. https://doi.org/10.1109/JIOT.2025.3530565.

172. Huang, W., Yu, A., Xu, Q., Sun, Q., Guo, W., Ji, S., Wen, B., and Qiu, C. (2024). Sea Ice Extraction via Remote Sensing Imagery: Algorithms, Datasets, Applications and Challenges. Remote Sens. *16*, 842. https://doi.org/10.3390/rs16050842.

173. Chen, W., Guan, N., Cheng, Q., Zhang, D., and Zhu, G. (2024). Experimental measurement and analytical method for critical temperature of

aircraft icing detection failure. Appl. Therm. Eng. *255*, 123980. https://doi.org/10.1016/j.applthermaleng.2024.123980.

174. Pohl, M. (2025). Wind tunnel and flight testing of a lamb wave-based ice accretion sensor. CEAS Aeronaut. J. *16*, 157–170. https://doi.org/10.1007/s13272-024-00781-3.

175. Dou, P., Li, Z., Dong, Z., and Xie, L.K. (2022). The optimization method of wing ice shape regulation based on flight dynamics characteristics. Sci. Rep. *12*, 18219. https://doi.org/10.1038/s41598-022-22824-7.

176. Shah, A., Niksan, O., Niknahad, F., Jain, M.C., Fuleki, D., Rasinarzabadi, F., and Zarifi, M.H. (2024). Unlocking Conformal Microwave Split Ring Resonant Sensors for In-Flight Ice Sensing. IEEE Trans. Aerosp. Electron. Syst. *60*, 525–536. https://doi.org/10.1109/TAES.2023.3328580.

177. Gonzalez, M., and Frövel, M. (2022). Fiber Bragg Grating Sensors ice detection: Methodologies and performance. Sensor Actuator Phys. *346*, 113778. https://doi.org/10.1016/j.sna.2022.113778.

178. Zhen, Z., Song, M., Zhu, X., Dai, X., Zhang, X., and Zhang, L. (2025). Experimental study on the effect of uneven temperature distribution of horizontal cold surface on 3D ice transparency in vertical ice-making process. Int. J. Refrig. *177*, 79–90. https://doi.org/10.1016/j.ijrefrig.2025.05.024.

179. Shao, K., Zhen, Z., Gao, R., Song, M., Zhang, L., and Zhang, X. (2024). Comparative experimental study of the effect of loading rate on the typical mechanical properties of bubble and clear ice cubes. Exp. Therm. Fluid Sci. *159*, 111264. https://doi.org/10.1016/j.expthermflusci.2024.111264.

180. Shao, K., Song, M., Zhang, X., Xu, C., Wang, Y., Hu, Y., and Wang, Z. (2024). Mechanical Analysis of the Critical Conditions for Trapping and Detachment of Microscale Air Bubbles on the Pure Water Freezing Front. Langmuir *40*, 25334–25343. https://doi.org/10.1021/acs.langmuir.4c03815.

181. Zhen, Z., Song, M., Cai, B., Zhang, X., Liu, Z., and Gao, R. (2025). Experimental and modeling studies on the growth characteristics of ice layers at different temperatures and salinities. Int. J. Heat Fluid Flow *115*, 109868. https://doi.org/10.1016/j.ijheatfluidflow.2025.109868.

182. Song, M., Gao, R., Dang, C., Shao, K., and Zhang, L. (2025). Solidification characteristics of two-dimensional water droplets. Droplet *4*, e70031. https://doi.org/10.1002/dro2.70031.

183. Shao, K., Song, M., Cai, B., Zhang, L., Pekař, L., and Zhang, X. (2024). Effects of Environmental Temperature and Trapped Air Bubbles on the Mechanical Properties of Ice Cubes. ACS Appl. Mater. Interfaces *16*, 63482–63494. https://doi.org/10.1021/acsami.4c12227.

184. Lan, W., Liu, X., Ye, K., Xie, M., and Chen, L. (2024). Comprehensive thermodynamic and economic analysis of an LNG cold energy recovery system using organic Rankine cycle and freezing-centrifugal desalination for power and water cogeneration. J. Clean. Prod. *461*, 142677. https://doi.org/10.1016/j.jclepro.2024.142677.

185. Wei, M., and Dai, F. (2021). Laboratory-scale mixed-mode I/II fracture tests on columnar saline ice. Theor. Appl. Fract. Mech. *114*, 102982. https://doi.org/10.1016/j.tafmec.2021.102982.

186. Hall, B., Johnson, S., Thomas, M., and Rampai, T. (2023). Review of the design considerations for the laboratory growth of sea ice. J. Glaciol. *69*, 953–965. https://doi.org/10.1017/jog.2022.115.

187. Magruder, L.A., Farrell, S.L., Neuenschwander, A., Duncanson, L., Csatho, B., Kacimi, S., and Fricker, H.A. (2024). Monitoring Earth's climate variables with satellite laser altimetry. Nat. Rev. Earth Environ. *5*, 120–136. https://doi.org/10.1038/s43017-023-00508-8.

188. Irwin, L.A.K., Coops, N.C., Anders, K., Mandlburger, G., and Winiwarter, L. (2025). Light detection and ranging of natural systems. Nat. Rev. Methods Primers *5*, 76. https://doi.org/10.1038/s43586-025-00446-3.

189. Wilson, S.F., Hogg, A.E., Rigby, R., Gourmelen, N., Nias, I., and Slater, T. (2025). Detection of 85 new active subglacial lakes in Antarctica from a decade of CryoSat-2 data. Nat. Commun. *16*, 8311. https://doi.org/10.1038/s41467-025-63773-9.

190. Yang, J., Gong, P., Fu, R., Zhang, M., Chen, J., Liang, S., Xu, B., Shi, J., and Dickinson, R. (2013). The role of satellite remote sensing in climate change studies. Nat. Clim. Chang. *3*, 875–883. https://doi.org/10.1038/nclimate1908.

191. Fusselman, J., Suarez, H., Amaireh, A., Perera, S., Zhang, Y.R., and Pratt, G. (2024). Miniature impulse radar sensor for snow and ice penetration sensing and weak layer detection. J. Appl. Remote Sens. *18*, 047501. https://doi.org/10.1117/1.JRS.18.047501.

192. Liu, W., Jin, T., Li, J., and Jiang, W. (2023). Adaptive Clustering-Based Method for ICESat-2 Sea Ice Retrieval. IEEE Trans. Geosci. Remote Sens. *61*, 1–14. https://doi.org/10.1109/TGRS.2023.3287909.

193. Shoja, S., Berbyuk, V., and Boström, A. (2018). Guided wave–based approach for ice detection on wind turbine blades. Wind Eng. *42*, 483–495. https://doi.org/10.1177/0309524X18754767.

194. Wagih, M., and Shi, J. (2021). Wireless Ice Detection and Monitoring Using Flexible UHF RFID Tags. IEEE Sens. J. *21*, 18715–18724. https://doi.org/10.1109/JSEN.2021.3087326.

195. Ji, H., Yang, C., Su, H., Qi, Z., Wang, Y., Cheng, E., and Hu, N. (2025). Multifunctional superhydrophobic film with comprehensive icing monitoring, anti-icing, and photothermal/electrothermal deicing properties. Prog. Org. Coat. *206*, 109337. https://doi.org/10.1016/j.porgcoat.2025.109337.

196. Azimi Dijvejin, Z., Jain, M.C., Kozak, R., Zarifi, M.H., and Golovin, K. (2022). Smart low interfacial toughness coatings for on-demand de-icing without melting. Nat. Commun. *13*, 5119. https://doi.org/10.1038/s41467-022-32852-6.